Antibiotic Persistence Emerges from Cell-State-Driven Transcriptional Reprogramming

Qiang Liu[1], Zehui Yu[1], Xiaoli Liu[1], Amy Iverson[2], Tyler Simmons[2], Jason W. Rosch[2,3], Peijun Ma[1,3]*

Affiliations

1. Department of Pharmacy and Pharmaceutical Sciences, St Jude Children's Research Hospital, Memphis, Tennessee, United States of America.

2. Department of Host-Microbe Interactions, St Jude Children's Research Hospital, Memphis, Tennessee, United States of America.

3. Center for Infectious Diseases Research, St Jude Children's Research Hospital, Memphis, Tennessee, United States of America.

* Corresponding Author. Email: peijun.ma@stjude.org

Abstract

Antibiotic persistence allows a subpopulation of bacterial cells to survive antibiotic treatment without acquiring resistance mutations, often contributing to treatment failure. Although many genes have been linked to persistence, their deletion rarely abolishes the phenotype, highlighting redundancy in persistence mechanisms. Moreover, the transient and heterogeneous nature of persister formation has made it difficult to resolve its molecular basis using bulk analyses. Here, we use bacterial single-cell RNA sequencing and functional assays in *Klebsiella pneumoniae* to demonstrate how transcriptional heterogeneity and redundancy in stress responses shape persistence outcomes. Using growth phase as a biologically meaningful axis of transcriptional variation, we reveal that even within an isogenic population, distinct transcriptional responses can be induced and co-contribute to survival. These responses are shaped by the cell's pre-treatment transcriptional state and the mechanism of antibiotic action. Genetic and environmental perturbations, such as *rpoS* deletion and nutrient supplementation, shift pre-treatment cell states and alter persistence frequencies. Our findings establish the biological significance of transcriptional heterogeneity shaped by pre-treatment cell states, providing a systems-

level framework for understanding persistence and suggesting strategies to enhance antibiotic efficacy by modulating cell states.

Introduction

Even within genetically identical populations, bacterial cells can differ in their physiological states. This phenotypic heterogeneity, whether pre-existing or stress-induced, is widely viewed as a bet-hedging strategy to ensure population survival under stress[1-3]. A prominent example is antibiotic persistence, where a small subpopulation of cells survives otherwise lethal antibiotic treatment, contributing to treatment failure, recurrent infections, and the evolution of resistance[4-8].

Antibiotic persisters can arise either as pre-existing cells that formed spontaneously or in response to other stresses, or as being induced upon antibiotic exposure[6,9,10]. For antibiotic-induced persisters, two steps are involved: first, the formation of persisters via transcriptional reprogramming in response to antibiotic stress; and second, the survival of persisters, often enabled by traits developed after the formation stage, such as metabolic dormancy, that help cells evade killing[9]. Thus, the trajectory of reprogramming induced upon antibiotic exposure is critical, as only certain directions lead to survival. However, how this direction is determined, how it unfolds across individual cells, and what factors govern it remain poorly understood.

This knowledge gap arises in part because the formation of persisters is a transient and dynamic process embedded within a phenotypically heterogeneous population. Bulk-level analysis often masks this heterogeneity, making it difficult to resolve the molecular mechanisms underlying persister formation[9]. For instance, previous studies have identified genetic pathways such as toxin-antitoxin systems, but deletion of these genes rarely eliminates persistence[11,12], suggesting the mechanisms involved are redundant, conditional, or embedded within broader regulatory networks. Stress response pathways, including the stringent response, the general stress response (RpoS), and the SOS response, have also been proposed as a general route to antibiotic persistence, pointing to a role for transcriptional reprogramming in survival[12-19]. However, these findings are based largely on bulk data,

leaving open the critical question of whether persistence arises through a single conserved transcriptional program or through multiple, divergent trajectories shaped by phenotypic heterogeneity. A central challenge is determining whether all cells follow a shared response to a given stress, or whether distinct subpopulations deploy parallel strategies to survive. Addressing this requires single-cell resolution to map the diversity of transcriptional responses underlying persistence[20].

The advent of bacterial scRNA-seq has enabled genome-wide profiling of transcriptional heterogeneity at single-cell resolution[21-26], offering new opportunities to dissect the dynamics of persister formation. A recent study applied this approach to identify a convergent persister-specific transcriptional state in *Escherichia coli*, but focused on pre-existing persisters formed before antibiotic exposure[27]. In contrast, understanding how antibiotics induce persistence, and whether different cell states follow distinct reprogramming paths under drug stress, requires systematic single-cell profiling during treatment.

Inspired by our recent discovery that meropenem, a β-lactam antibiotic that inhibits cell-wall synthesis, induces heterogeneous molecular responses including a subpopulation enriched for persisters[23], we hypothesized that persister formation can be initiated through diverse mechanisms simultaneously triggered by antibiotics. Since antibiotic persistence varies across bacterial growth phases, with stationary-phase cells being the most tolerant[28,29], we further hypothesized that cells at different growth phases exhibit distinct antibiotic responses that drive different levels of persistence.

To test these hypotheses, we focused on *Klebsiella pneumoniae*, a clinically important pathogen associated with recurrent and multidrug-resistant infections[30]. We used scRNA-seq to profile its transcriptional responses to antibiotics across lag, exponential, and stationary phases, leveraging growth phase as a biologically meaningful axis of variation in pre-treatment cell states. Our findings reveal that antibiotic survival can be achieved through divergent transcriptional reprogramming pathways within the same isogenic population, shaped by both the cell's pre-treatment transcriptional state and the antibiotic's mechanism of action. Moreover, we show that altering the pre-treatment cell states, through genetic or nutrient perturbation, can modulate persistence levels.

Together, these results demonstrate how pre-treatment cell states shape transcriptional reprogramming and survival during antibiotic exposure, providing direct evidence for the biological significance of transcriptional heterogeneity in antibiotic survival and persistence. This work establishes: (i) a systems-level framework that provides mechanistic insight into why persistence cannot be eliminated by targeting single genes; (ii) a potential strategy to enhance antibiotic efficacy by modulating bacterial cell states; and (iii) a foundation for broader single-cell profiling across bacterial species and for *in vivo* characterization of heterogeneity and drug responses.

Results

Profiling pre-treatment cell states at various growth phases that are linked to different levels of persistence

To profile transcriptional reprogramming across bacterial growth phases, we first mapped the "pre-treatment cell states" using scRNA-seq in cultures prior to antibiotic treatment. We used an optimized version of BacDrop protocol (BacDrop_V2) with improved coverage (see Methods and Supplementary Fig. 1). We define "cell state" as a transcriptomic profile representing a cell's regulatory and physiological status, serving as a proxy for its proteomic and metabolic activity. Although transcriptomes do not fully capture cellular function, they provide a predictive snapshot of pathways involved in stress adaptation and survival. While bacterial cultures are traditionally categorized by bulk growth phases, it remains unclear whether these phases represent uniform physiological states or heterogeneous mixtures of distinct cell states. This distinction is critical, as population-level measurements obscure the single-cell heterogeneity that may shape antibiotic response and survival.

To define bacterial cell states at single-cell resolution before antibiotic exposure, we performed scRNA-seq on a clinical isolate of *K. pneumoniae* MGH66 cultures at early lag (10 minutes post-transfer to fresh medium, LAG10), exponential (EXP), and stationary phases (STA) under unperturbed conditions (Fig. 1a). To minimize carryover from the inoculum, cultures were serially diluted three times before sampling EXP cells (~2 hours after dilution into fresh medium). Transcriptional cell states were

identified using unsupervised clustering followed by pathway enrichment analysis, enabling functional annotation of each cluster (Fig. 1b,c, Supplementary Fig. 2). While we refer to these as discrete "states," they likely lie along a continuum and represent overlapping transcriptional programs dynamically weighted over time. To ensure robust annotation and reproducibility, we included two biological replicates per condition and excluded clusters found in only one replicate.

We identified eight reproducible transcriptional cell states across three growth phases, with each phase characterized by a dominant expression profile (Fig. 1c–e, Supplementary Tables 1–3). At the LAG10 phase, ~70% of cells exhibited a ribosome biogenesis program. During the EXP phase, ~60% of cells exhibited relative enrichment of respiration-associated transcripts compared to other states, while ~10% retained a ribosome-associated transcriptional profile. By the STA phase (16 hours post-dilution), ~60–70% of cells adopted a starvation-adaptation state, marked by *rpoS* and biofilm gene upregulation. These findings reveal structured heterogeneity within bacterial growth phases, with transcriptional profiles correlating with differential antibiotic survival: at the population level, stationary-phase cells showed the highest persistence, while exponential-phase cells were the most susceptible (Fig. 1f). Of note, to maintain analytical consistency, we applied the same minimum gene-detection cutoff across all three growth phases. However, stationary-phase bacteria are known to yield substantially fewer detectable transcripts per cell, a biological property reported in multiple bacterial single-cell studies, including *E. coli* [21,27] and *Bacillus subtilis*[22]. As a result, fewer stationary-phase cells passed this uniform filtering threshold (Supplementary Table 1). To assess whether this difference affected state identification, we performed an additional analysis in which the minimum gene-detection cutoff was specifically relaxed for stationary-phase cells to achieve comparable cell numbers to the LAG10 and EXP phases. This analysis recovered the same major transcriptional states and overall structure, yielding results consistent with those obtained using a uniform cutoff (Supplementary Fig. 3; Supplementary Table 1). We note that despite this validation, stationary-phase sampling depth remains

124 lower than that of lag and exponential phases, which may limit detection of rare transcriptional
125 subpopulations.

126 These results demonstrate that bacterial growth phases comprise transcriptionally distinct cell states
127 that are associated with functional differences in antibiotic survival. These transcriptional states capture
128 dominant transcriptional programs that are differentially enriched across growth phases, reflecting shifts
129 in physiological emphasis rather than mutually exclusive or sequential activation of individual processes
130 (Fig. 1g). Notably, a “cell division” state was identified across all three growth phases (Fig. 1c,d),
131 marked by core division genes such as *ftsA* (Fig. 1e). However, closer inspection revealed that cells
132 within this state exhibited distinct marker profiles associated with ribosome biosynthesis or respiration,
133 reflecting their respective growth phases. In subsequent experiments, we use these growth phase-
134 defined populations, each with a characteristic distribution of cell states, as a biologically meaningful
135 axis to test how pre-treatment cell states influence transcriptional reprogramming and persistence
136 under antibiotic exposure.

137 **Meropenem induced heterogeneous transcriptional reprogramming across growth phases**

138 We next profiled the transcriptional reprogramming induced by meropenem across bacterial growth
139 phases characterized by distinct cell state structures. Using the same sampling scheme as in Fig. 1a,
140 we exposed *K. pneumoniae* cultures from LAG10, EXP, and STA phases to meropenem at a lethal
141 concentration (40× of minimal inhibitory concentration (MIC)). For the LAG10 and EXP cells, we
142 collected samples when ~40–60% of cells had been killed based on quantification of colony forming
143 unit (CFU) on LB agar plates. For STA cells that showed high-level antibiotic tolerance (Fig. 1f), we
144 collected cells at 15 minutes after antibiotic exposure.

145 Upon meropenem exposure, scRNA-seq results revealed that three new cell states emerged: 1) the
146 heat shock response that is marked by upregulation of *dnaK*, *groES*, and *groEL*; 2) *osmB* upregulation
147 accompanied with induced expression of two small RNAs *csrB* and *csrC*; 3) and a cell state with both
148 iron transport and heat shock upregulation (Fig. 2a–c, Supplementary Fig. 4, Supplementary Tables 4,

149 5). Across all three states, we observed induction of *lpp* (annotated as *lpp1* in *K. pneumoniae* MGH66
150 genome), which encodes Braun's lipoprotein, the major outer membrane protein that covalently links
151 the outer membrane to the peptidoglycan layer[31], suggesting a shared response involving envelope
152 stabilization under stress (Fig. 2c).

153 Although these three new cell states were observed in cells treated with meropenem across all growth
154 phases, major transcriptional responses differed dramatically by growth phase (Fig. 2d,e). In LAG10
155 cells treated with meropenem, 79.6–94.7% of the population activated the heat shock response (Fig.
156 2d,e). Given that LAG10 cells were actively engaged in ribosome biogenesis (Fig. 2e), this response
157 likely mitigates proteotoxic stress from misfolded or stalled translation products. In addition, 0.1–1.0%
158 of LAG10 cells upregulated *osmB* and 2% of cells showed high-level expression of both iron transport
159 genes and heat shock response.

160 EXP-phase cells also showed a heterogenous reprogramming under meropenem treatment, consistent
161 with our previous findings[23]. Approximately 34% upregulated *osmB*, while smaller subpopulations
162 activated starvation adaptation (2.7–3.1%), heat shock programs (0.8–1.0%), or both heat shock and
163 iron transport responses (1.2–1.5%) (Fig. 2d,e; Supplementary Table 4). Of note, a starvation-
164 adaptation population was also detected in untreated EXP-phase cells (1.6%) (Fig. 1d), suggesting that
165 these cells may emerge spontaneously during growth and are subsequently enriched, or induced,
166 under antibiotic stress. Given that EXP cultures were serially diluted prior to sampling (Fig. 1a), these
167 cells are unlikely to represent carryover from the inoculum because only 0.2–0.8% of untreated LAG10-
168 phase cells were in the starvation adaptation state (Fig. 1d, Supplementary Table 1).

169 STA cells showed high-level antibiotic tolerance and had been considered as dormant cells (Fig. 1f).
170 However, unexpectedly, we observed that 8.9–10% of STA cells upregulated *osmB*, 6.8–8.1% of STA
171 cells showed heat shock response, and 1.9–2.1% of STA cells showed both iron transport and heat
172 shock responses under meropenem treatment (Fig. 2d,e; Supplementary Table 4). Notably, all of these
173 responding cells upregulated *lpp1* (Fig. 2c). In addition, we also observed a significant reduction of cells

174 in the starvation adaptation state and a 20-fold increase of cells in the iron transport state. Similarly to
175 the untreated condition, stationary-phase cells treated with meropenem yielded fewer cells passing
176 quality control when a uniform minimum gene-detection cutoff was applied. To assess whether this
177 affected transcriptional state identification, we performed an additional analysis in which the minimum
178 gene-detection threshold was specifically relaxed for STA cells. This analysis recovered transcriptional
179 states and overall structure consistent with the primary analysis, indicating that the conclusions are
180 robust to differences in cell number and detection depth (Supplementary Fig. 5; Supplementary Table
181 4). Experimentally, using a GFP reporter driven by the native *lpp1* promoter, we validated that STA cells
182 indeed upregulated *lpp1* (Supplementary Fig. 6), confirming that meropenem triggers transcriptional
183 reprogramming in a subset of STA cells under our experimental conditions.

184 Together, these results demonstrate that meropenem induces heterogeneous transcriptional responses,
185 with profiles varying by growth phase. The dominant responses observed, such as heat shock in
186 LAG10 cells and *osmB*-upregulation in EXP cells, highlight the influence of pre-treatment cell states on
187 transcriptional reprogramming. LAG10, EXP, and STA populations differ not only in baseline physiology
188 but also in how they reprogram under stress, underscoring the importance of growth-phase-specific cell
189 states in shaping antibiotic responses.

190 **Antibiotic survival is enhanced from multiple mechanisms simultaneously induced by**
191 **meropenem**

192 The observation that multiple stress responses were induced motivated us to test the functional
193 relevance of the observed transcriptional heterogeneity. Specifically, in EXP-phase cells treated with
194 meropenem, three transcriptional responses, including *osmB* upregulation accompanied with
195 upregulation of *csrB* and *csrC*, starvation adaptation marked by high-level expression of *rpoS*, and heat
196 shock response, were identified as candidate survival-associated programs.

197 To assess their relationship to antibiotic survival, we measured survival rates using GFP reporter strains
198 driven by the *osmB* or *rpoS* promoter. After meropenem exposure, EXP-phase cells were sorted into

199 high- and low-GFP populations (top/bottom 10%), excluding dead cells using DAPI (Fig. 2f,
200 Supplementary Fig. 7a–e). High expressers (OsmB.high or RpoS.high) exhibited a 4 to 10-fold increase
201 in survival compared to low expressers and unsorted controls (Fig. 2g). To address the possibility that
202 higher GFP signal reflects non-growing cells accumulating GFP non-specifically, we included a control
203 reporter strain in which GFP is driven by the promoter of a housekeeping gene (*fusA*), whose
204 expression is high and relatively uniform across the population with minimal cell-to-cell heterogeneity
205 under our experimental conditions. Using this control, we show that sorting FusA.high and FusA.low
206 cells does not result in a significant difference in survival, indicating that the survival advantage
207 observed for stress-responsive reporters is not due to nonspecific GFP accumulation (Supplementary
208 Fig. 7g,h).

209 To examine whether activation of the heat-shock response broadly modulates survival, we pre-treated
210 EXP cells at 42°C for 30 minutes prior to antibiotic exposure. Heat-shocked EXP cells showed
211 reproducible increase in survival following meropenem treatment (Fig. 2h), consistent with the
212 protective role of heat shock observed in LAG10 cells. This pre-treatment likely primes cells to mitigate
213 proteotoxic stress, potentially explaining the greater tolerance of LAG10 cells relative to untreated EXP
214 cells (Fig. 1f).

215 Together, these results show that meropenem treatment induces divergent transcriptional responses
216 that collectively modulate survival outcomes (Fig. 2i). This redundancy provides a potential explanation
217 for why perturbation of individual genes often fails to eliminate surviving cells. While these experiments
218 do not establish direct causal relationships between specific transcriptional states and persistence at
219 the single-cell level, they demonstrate that transcriptional heterogeneity shapes antibiotic survival in a
220 growth-phase-dependent and context-specific manner, setting the stage for the emergence of
221 persistence under sustained antibiotic stress.

222 **Divergent transcriptional reprogramming induced across mechanistically distinct antibiotics**

223 The findings under meropenem treatment raise another critical question: can divergent transcriptional
224 reprogramming also be triggered by antibiotics with distinct cellular targets, such as those inhibiting
225 DNA replication? To address this question, we treated *K. pneumoniae* cells from LAG10, EXP, and STA
226 phases with a lethal concentration (80x MIC) of ciprofloxacin, a DNA synthesis-inhibiting antibiotic, and
227 profiled their reprogramming by scRNA-seq. Ciprofloxacin and related fluoroquinolones are known to
228 induce the SOS response[32], centered on *recA* and downstream DNA repair genes.

229 Under ciprofloxacin treatment, unsupervised clustering revealed four new transcriptional cell states
230 characterized by *recA* upregulation (Fig. 3a–c, Supplementary Fig. 8, Supplementary Tables 6,7). While
231 all four clusters shared activation of the SOS response, they were transcriptionally distinct due to
232 differences in co-regulated stress response programs (Fig. 3c). We named these clusters based on
233 their predominant cell-of-origin: SOS_EXP and three SOS_LAG clusters. The SOS_EXP cluster co-
234 upregulated canonical heat shock genes including *dnaK*, *groL*, and *groES*, in addition to *recA*. In
235 contrast, SOS_LAG clusters upregulated *recA* and *recN*, a gene involved in recombination repair of
236 DNA double stranded breaks, but did not activate the heat shock program at the time of sampling.
237 Among the SOS_LAG clusters, the degree of *recN* upregulation varied, with SOS_LAG1 showing the
238 highest expression (Fig. 3c).

239 These SOS clusters were not exclusive to a single growth phase but appeared across all three (Fig.
240 3d,e, Supplementary Table 6). However, their relative abundance and transcriptional profiles were
241 strongly phase dependent. In EXP-phase cells, approximately 53.1–59.3% co-induced the SOS and
242 heat shock responses, and ~12.6–14.4% upregulated *recA* and *recN* without activating heat shock
243 genes. Flow cytometry using GFP reporters confirmed *recA* and heat shock gene induction in EXP
244 cells, validating their co-upregulation at the EXP growth phase under ciprofloxacin treatment (Fig. 3f,
245 Supplementary Fig. 9). In contrast, ~55% of LAG10 cells upregulated *recA* and *recN* without heat shock
246 gene induction (SOS_LAG). Similar to the response observed under meropenem, STA cells,
247 traditionally regarded as dormant, displayed minimal but detectable transcriptional activity under

248 ciprofloxacin treatment. Most responding cells exhibited *recA* activation together with weak *recN*
249 upregulation within the SOS_LAG3 cluster. Similarly, for ciprofloxacin-treated samples, STA cells
250 yielded fewer cells passing quality control under a uniform gene-detection cutoff; relaxing this threshold
251 for STA cells recovered transcriptional states consistent with the primary analysis (Supplementary Fig.
252 10; Supplementary Table 6). Using a GFP reporter driven by the native *recA* promoter, we validated
253 that a subset of STA cells indeed upregulated *recA* (Supplementary Fig. 11), confirming that
254 ciprofloxacin also induces transcriptional reprogramming in these cells under our experimental
255 conditions.

256 Together, these results demonstrate that while both LAG10 and EXP cells activate the SOS response to
257 ciprofloxacin, the co-activation of additional stress programs diverges between phases (Fig. 3g). EXP
258 cells prominently co-induce canonical heat shock genes, whereas LAG10 cells primarily co-induce the
259 downstream DNA repair gene *recN*. This divergence may reflect phase-specific differences in
260 reprogramming capacity, transcriptional burden, or stress thresholds that are rooted in their distinct pre-
261 treatment physiological states: EXP cells are predominantly engaged in respiration, while LAG10 cells
262 are characterized by active ribosome biosynthesis (Fig. 3g). While these data reveal clear phase-
263 dependent heterogeneity within the SOS response, the functional consequences of this heterogeneity
264 for survival under ciprofloxacin treatment were not directly tested and remain an open question.

265 Combined with our findings under meropenem treatment, these results support a general principle:
266 antibiotics can induce divergent transcriptional reprogramming within and across growth phases,
267 shaped not by drug mechanism alone, but by the interplay between a cell's pre-treatment
268 transcriptional state and the antibiotic's mode of action. Crucially, this divergent reprogramming is
269 functionally important for survival, as demonstrated in EXP cells under meropenem treatment (Fig.
270 2g,h), and likely applicable to ciprofloxacin-induced states as well. Notably, complementary flow
271 cytometry experiments across a range of antibiotic concentrations indicate that the same stress-
272 responsive transcriptional programs are induced under lower, more clinically relevant doses, although

273 their timing and magnitude are concentration dependent (Supplementary Fig. 12). Our findings
274 therefore provide a systems-level view of antibiotic survival at the early stage of persister formation,
275 emphasizing how pre-treatment cell states shape transcriptional responses and survival, and pointing
276 to new opportunities to predict or manipulate bacterial outcomes by modulating cell states.

277 ***RpoS* deficiency alters levels of antibiotic persistence via modulation of pre-treatment cell**
278 **states**

279 Building on our observations in wild-type *K. pneumoniae*, we hypothesized that antibiotic persistence
280 levels could be altered by perturbing the pre-treatment cell states prior to drug exposure. To test this,
281 we deleted *rpoS*, a conserved sigma factor that regulates general stress responses across bacterial
282 species and has been implicated as a key gene in antibiotic persistence[12,13].

283 Consistent with previous findings[18], *rpoS* deletion significantly reduced persistence in STA-phase cells.
284 Notably, the same deletion markedly increased survival during the LAG10 phase under both
285 meropenem and ciprofloxacin treatment, while having no effect in EXP-phase cells (Fig. 4a). This
286 pattern was reproduced in *E. coli* K-12, with *rpoS* deletion decreasing persistence in STA cells,
287 increasing survival in LAG cells, and showing no effect in EXP cells (Supplementary Fig. 13), indicating
288 that the phenomenon is not species-specific. Although enhanced persistence upon *rpoS* deletion has
289 been documented in *E. coli* and *Pseudomonas aeruginosa*[16], the mechanisms underlying these
290 contrasting, growth phase-dependent outcomes have remained unclear.

291 To investigate the molecular basis of this phase-specific effect, we profiled the transcriptional cell states
292 of *rpoS*-deficient (Δ*rpoS*) and wild-type (WT) strains at the LAG10 and EXP phases using scRNA-seq.
293 Although Δ*rpoS* cells exhibited markedly reduced antibiotic persistence in STA phase, attempts to
294 profile this condition by scRNA-seq yielded insufficient numbers of mRNA/cell and low cell recovery for
295 inclusion in the final analysis, and we therefore restrict the Δ*rpoS* dataset to LAG10 and EXP phases.
296 At the LAG10 phase, WT cells initiated ribosome biogenesis, as previously observed. In contrast,
297 approximately 50% of Δ*rpoS* cells exhibited strong upregulation of heat shock genes, including *dnaK*,

298 *groES*, and *groEL* (Fig. 4b–d, Supplementary Fig. 14, Supplementary Tables 8,9). Although *rpoS* is well
299 known for mediating the transition from exponential to stationary phase, it also plays a role during the
300 shift from stationary to lag phase by regulating pathways such as iron uptake[33,34]. Our results suggest
301 that in the absence of *rpoS*, cells may compensate by activating the heat shock response to support the
302 transition from dormancy to active growth. Together with our earlier observation that heat shock
303 activation enhances antibiotic survival, this provides a potential mechanistic explanation for the
304 increased survival of Δ*rpoS* cells in the LAG phase.

305 To capture the temporal dynamics of this reprogramming by *rpoS* deletion, we also profiled Δ*rpoS* cells
306 30 minutes post-dilution (LAG30). At this point, their transcriptomes more closely resembled WT LAG10
307 cells, although ~10% of cells retained a heat shock signature, indicating delayed or incomplete
308 adaptation (Fig. 4b,c). By the EXP phase, Δ*rpoS* and WT cells showed similar transcriptional profiles
309 dominated by respiration (Fig. 4b,c), consistent with their comparable levels of antibiotic persistence in
310 this phase.

311 Altogether, these findings demonstrate that perturbation of *rpoS* can alter pre-treatment cell states, a
312 potential mechanism through which the level of antibiotic persistence is modulated. While RpoS is
313 classically associated with stress protection and has been implicated in persistence, our results reveal
314 that its effects are strongly context dependent. In the LAG phase, RpoS facilitates the transition from
315 starvation adaptation to ribosome biogenesis; its absence instead triggers a heat shock response and
316 paradoxically increases persistence (Fig. 4e). These results provide a potential mechanistic basis for
317 the growth phase-specific effects of RpoS on persistence and underline the limitations of gene-targeted
318 approaches for modulating antibiotic persistence.

319 **Nutrient shift reprograms stationary phase cells and restores antibiotic sensitivity**

320 Having shown that genetic perturbation of pre-treatment cell states alters antibiotic survival, we
321 hypothesized that non-genetic interventions, such as nutrient shifts, could similarly modulate

322 transcriptional states and sensitize tolerant cells. This concept has been proposed by prior work
323 showing that certain carbon sources can activate aminoglycoside uptake and killing of *E. coli* persisters
324 via restoration of proton motive force[35]. However, these effects were largely limited to aminoglycosides
325 and varied depending on bacterial species and nutrient type. Moreover, past efforts focused on bulk
326 phenotypes and did not investigate how nutrient supplementation alters the transcriptional landscape or
327 interacts with antibiotics beyond aminoglycosides. Here, we tested whether specific nutrient inputs
328 could shift bacterial cell states and alter antibiotic survival under meropenem and ciprofloxacin. If
329 successful, this strategy could provide a generalizable way to enhance antibiotic efficacy by shifting
330 bacterial populations into more vulnerable physiological states.

331 To evaluate this, we focused on STA cells, which exhibited the highest levels of antibiotic tolerance. We
332 screened a variety of nutrients, including carbon sources, nitrogen sources, amino acids, and metals,
333 by supplementing them individually into spent medium (filtered from overnight MHB cultures), and
334 assessed survival under meropenem and ciprofloxacin treatment (Supplementary Fig. 15). For
335 meropenem-treated STA cells, glucose supplementation reduced survival by roughly 1000 folds after 4-
336 hour treatment (Fig. 5a). For ciprofloxacin-treated STA cells, ferrous sulfate ($FeSO_4$) reduced survival
337 by approximately 30–100 folds after 4-hour treatment (Fig. 5b). Notably, glucose had no effect under
338 ciprofloxacin, and $FeSO_4$ had no effect under meropenem (Supplementary Fig. 15), suggesting that
339 these two interventions sensitize cells through distinct mechanisms. Importantly, we confirmed that
340 glucose or $FeSO_4$ alone did not affect survival in the absence of antibiotics (Supplementary Fig. 16),
341 indicating that their effects depend on the antibiotic used.

342 To uncover how glucose sensitizes stationary-phase cells to meropenem, we performed scRNA-seq on
343 STA cells transferred into spent medium supplemented with 20 mM glucose and sampled them at 2 and
344 4 hours post-transfer. By 2 hours, cells had re-entered growth, exhibiting active DNA replication and cell
345 wall synthesis (Fig. 5c–e; Supplementary Fig. 17; Supplementary Tables 10,11). By 4 hours, ~80% of
346 cells transitioned into a transcriptional state of carbon overflow[36,37], characterized by mixed metabolic

347 reprogramming and stress responses (Fig. 5c–e), including upregulation of fermentation genes,
348 glycolysis genes, anaerobic respiration genes, and stress response pathways (Fig. 5f, Supplementary
349 Tables 10,11). Because replicates differed substantially in recovered cell numbers for this condition, we
350 restrict interpretation to the predominant transcriptional programs rather than quantitative estimates of
351 rare states. These findings indicate that glucose supplementation drives a growth trajectory distinct
352 from that induced by fresh medium, which primarily activates aerobic respiration (Fig. 1g). Instead,
353 under carbon excess but limitation in other nutrients, cells engage alternative metabolic programs to
354 support growth, rendering them more susceptible to meropenem-mediated killing.

355 We next investigated how $FeSO_4$ enhances ciprofloxacin killing. Unlike glucose supplementation, which
356 allowed us to profile transcriptional states using scRNA-seq, $FeSO_4$-treated STA cells exhibited low
357 RNA content, and we were unable to recover enough high-quality cells for single-cell analysis. We
358 therefore turned to bulk RNA-seq, which offers greater sensitivity. In the absence of antibiotic, $FeSO_4$
359 supplementation led to robust upregulation of the *arn* operon, a pathway involved in lipid A modification
360 and known to respond to Fe^{2+}. We also observed significant downregulation of ferric (Fe^{3+}) iron uptake
361 systems, suggesting a shift in iron homeostasis (Fig. 5g,h; Supplementary Tables 12,13). Under
362 ciprofloxacin treatment, these transcriptional changes persisted, along with a marked induction of the
363 SOS response (Fig. 5g,h). The downregulation of Fe^{3+} uptake pathways suggests intracellular Fe^{3+}
364 accumulation, potentially resulting from Fe^{2+} oxidation following supplementation. We thus
365 hypothesized that the conversion of Fe^{2+} to Fe^{3+} via Fenton chemistry generates reactive oxygen
366 species (ROS), thereby potentiating antibiotic lethality[38]. Supporting this model, the addition of thiourea,
367 a ROS scavenger, attenuated the killing effect (Fig. 5i). Notably, thiourea alone did not affect
368 ciprofloxacin-mediated killing, suggesting that in the absence of Fe^{2+}, ciprofloxacin acts through a ROS-
369 independent mechanism in STA cells. Together, these results reveal a mechanistic basis for how $FeSO_4$
370 potentiates ciprofloxacin activity against antibiotic-tolerant STA cells through Fe^{2+}-driven oxidative
371 stress that synergizes with drug-induced damage.

372 Altogether, these results demonstrate that nutrient shifts can serve as an effective strategy to sensitize
373 antibiotic-tolerant cells. Notably, the mechanism of sensitization depends on both the antibiotic used
374 and how nutrient-induced transcriptional changes intersect with the drug's mode of action (Fig. 5j).

375 **Discussion**

376 By applying bacterial scRNA-seq, we were able to directly profile the heterogeneous responses that
377 linked to antibiotic survival, providing insight into early programs that may precede persister formation.
378 This approach revealed that pre-treatment cell states play a critical role in shaping transcriptional
379 reprogramming profiles, which in turn determine survival outcomes under antibiotic stress. Using
380 growth phase as a biologically meaningful axis of heterogeneity, we found that *K. pneumoniae* cells can
381 engage multiple, distinct survival pathways simultaneously. These divergent reprogramming pathways
382 are largely dictated by the interplay between a cell's pre-treatment transcriptional state and the
383 antibiotic's mechanism of action. Genetic and environmental perturbations, such as *rpoS* deletion and
384 nutrient supplementation, shifted pre-treatment cell states and thereby redirected reprogramming and
385 altered persistence frequencies. Notably, the effect of *rpoS* deletion was conditional on growth phase,
386 illustrating how redundancy and plasticity within stress responses buffer against single-gene
387 perturbations. Together, these results provide direct mechanistic evidence linking pre-treatment cell
388 states to antibiotic-induced transcriptional reprogramming and persistence, framing persistence as a
389 systems-level property shaped by heterogeneity and redundancy.

390 **Profiling bacterial heterogeneity and its biological significance**

391 Our analysis revealed that *K. pneumoniae* cells exposed to antibiotics did not respond uniformly but
392 instead followed multiple transcriptional responses, each associated with distinct survival outcomes.
393 For example, under meropenem treatment, STA-phase cells reprogrammed minimally and survived;
394 LAG-phase cells activated heat shock; and EXP-phase cells diversified into subpopulations that
395 engaged upregulation of *osmB*, starvation adaptation, or heat shock responses. These divergent

396 responses were not random but constrained by baseline transcriptional states. Importantly, multiple
397 responses could support cell survival within the same isogenic population at the same growth phase
398 (Fig. 2g,h), indicating that survival is not determined by a single conserved program. Moreover, deletion
399 of *rpoS* had conditional effects on persistence (Fig. 4a), illustrating that no single gene is determinative
400 and that redundancy within stress responses contributes to survival. Together, these findings
401 demonstrate the biological significance of transcriptional heterogeneity shaped by pre-treatment states,
402 explaining why persistence remains robust across conditions and resistant to single-gene perturbations.

403 A limitation of the current study is reduced sampling depth for stationary-phase cells, particularly under
404 antibiotic treatment, reflecting the low RNA content of these cells and current technical constraints of
405 bacterial scRNA-seq. While additional analyses with relaxed filtering thresholds recovered consistent
406 transcriptional states, rare subpopulations may remain undetected. Similarly, stationary-phase cells
407 under the $FeSO_4$-treated conditions and in the Δ*rpoS* strain exhibited markedly reduced numbers of
408 detected genes per cell despite comparable sequencing depth, and we were unable to recover
409 sufficient cells for downstream analysis. These observations are consistent with biological states
410 characterized by low recoverable mRNA, although technical sensitivity remains a general challenge for
411 bacterial scRNA-seq. Further advances in sensitivity will be required to resolve such low-transcription
412 states.

413 While growth phase served as a practical axis of heterogeneity in this study, we also observed
414 substantial transcriptional variation within each phase. The functional relevance of this within-phase
415 heterogeneity remains unresolved. Addressing it will require lineage tracing and advanced
416 computational modeling that directly link pre-treatment cell state to cell fate[39], approaches that are not
417 yet available for bacterial scRNA-seq. Although we defined transcriptional states as discrete clusters,
418 these likely lie along a continuum of regulatory and physiological transitions. Our scRNA-seq analysis
419 offers snapshots of this landscape, but a fuller understanding of persistence will require time-resolved

420 approaches that can capture continuous trajectories and dynamic reprogramming at single-cell
421 resolution.

422 **Modulating cell states to overcome persistence**

423 Our findings demonstrate that rationally shifting bacterial cell states can reprogram transcriptional
424 states and reshape antibiotic susceptibility. While previous studies have proposed targeting specific
425 genes or pathways to overcome persistence, our results caution against such gene-centric approaches.
426 For example, deletion of *rpoS*, a conserved global stress response regulator, produced divergent
427 effects on persistence depending on growth phase (Fig. 4a). This context-dependent behavior
428 underscores the limitations of single-gene interventions and supports the need for a systems-level
429 strategy to modulate bacterial cell states.

430 Rather than focusing on individual persistence factors, we propose that interventions should aim to
431 reshape the overall transcriptional landscape to drive bacterial populations into vulnerable states.
432 Environmental perturbations, such as nutrient supplementation, may offer one such route. While further
433 work is needed to translate this strategy into clinical settings, cell-state-based modulation may offer a
434 broadly effective route to overcome antibiotic persistence.

435 **Toward a broader and *in vivo* understanding of antibiotic persistence**

436 Our findings, while derived from a clinical isolate of *K. pneumoniae* from a urinary tract infection, a
437 context frequently associated with recurrence and persistence, likely reflect conserved principles that
438 extend beyond this strain and species. The transcriptional states we identified, both before and after
439 antibiotic exposure, involve core metabolic pathways and conserved stress responses such as the
440 RpoS-mediated general stress response and the SOS response. These are well-characterized
441 pathways with established roles in persistence across multiple species. For instance, the conditional
442 effect of *rpoS* deletion on persistence was not only observed in *K. pneumoniae* (Fig. 4a) but also

443 validated in *E. coli* (Supplementary Fig. 13), and is consistent with previous reports in *E. coli* and
444 *Pseudomonas*[16], suggesting this phenomenon is not strain-specific. Together, these findings suggest
445 that our observations are not unique to a particular isolate but instead represent broadly relevant cell-
446 state features with implications for persistence across species.

447 Our experiments were conducted under well-controlled *in vitro* conditions, enabling precise dissection
448 of how pre-treatment transcriptional states shape antibiotic responses. In contrast, *in vivo* environments
449 introduce additional complexity, including spatial organization, immune pressure, and polymicrobial
450 interactions, that may reshape bacterial physiology and cell-state dynamics. Therefore, interpreting
451 bacterial single-cell responses in such complex environments requires robust reference frameworks.
452 Moving forward, the cell-state markers defined here provide a foundational resource for annotating
453 bacterial states *in vivo* and for generating mechanistic hypotheses about persistence. Together, this
454 work offers both mechanistic insight and a technical roadmap for future studies across diverse
455 pathogens and infection contexts, advancing efforts to rationally reprogram bacterial cell states and
456 improve antibiotic efficacy.

457 **Methods**

458 **Bacterial strains and growth conditions**

459 All scRNA-seq experiments are listed in Supplementary Table 14. The bacterial strains used in this
460 study are listed in Supplementary Table 15. *K. pneumoniae* MGH66[40] served as the parental strain for
461 generating derivatives. *K. pneumoniae* strains were routinely grown in Mueller-Hinton Broth (MHB) at
462 37°C with shaking at 220 rpm. Competent cells of *E. coli* NEB 10-beta, employed for plasmid cloning
463 and propagation, were purchased from New England Biolabs (NEB). *E. coli* K-12 wild-type and its
464 derived Δ*rpoS* mutant strains were obtained from the Keio collection[41].

465 To investigate transcriptional heterogeneity across bacterial growth phases and with antibiotic stress, *K.*
466 *pneumoniae* cells were collected at distinct growth stages for scRNA-seq. To obtain lag-phase cells,

467 stationary-phase cultures were diluted 1:100 into 30-ml fresh MHB and grown at 37°C for 10 min before
468 harvesting. For exponential-phase cells, stationary-phase cultures were first diluted 1:100 into fresh
469 MHB and grown to an OD_{600} of 0.2. The cultures were then subjected to two additional rounds of 1:100
470 back-dilution into 30-ml fresh MHB, each time grown to an OD_{600} of 0.2. Cells were collected after the
471 final dilution when the OD_{600} reached 0.2. Stationary phase cells were obtained by inoculating glycerol
472 stocks into fresh MHB and incubating for approximately 16 hours. The resulting populations were
473 designated as lag-phase (LAG10), exponential-phase (EXP), and stationary-phase (STA) cells,
474 respectively. To characterize the transcriptional profiles of nutrient-shifted STA cells, STA cultures were
475 diluted 1:100 into nutrient-spent medium supplemented with 20 mM glucose and grown for 2 or 4 hours.
476 Nutrient-spent medium was obtained from the supernatant of overnight cultures and sterilized using a
477 0.22 μm vacuum driven filtration system (Millipore, S2GPU02RE). For the antibiotic-treated samples,
478 cells from each growth phase were incubated with 2 μg/ml meropenem (Sigma-Aldrich, 1392454) or 2.5
479 μg/ml ciprofloxacin (Sigma-Aldrich, 17850) at 37°C with shaking for the indicated time periods. After
480 antibiotic exposure, cells were collected by centrifugation at 4°C for 15 min at 4,500g and immediately
481 fixed using 4% formaldehyde in PBS, incubate overnight at 4°C, then processed for subsequent
482 scRNA-seq experiments.

483 **Cell fixation and permeabilization**

484 The scRNA-seq protocol used in this study (BacDrop_V2) was optimized by replacing the second-
485 round barcoding strategy from BacDrop[23] with the thermo-ligation based in-droplet barcoding, as
486 validated and described by previous studies[24,42]. Details of the workflow are shown in Supplementary
487 Fig. 1. Key reagents or kits used in this study are listed in Supplementary Table 16.

488 The cell fixation and permeabilization were performed following our previously established protocol.
489 Briefly, Bacterial cells (~10^9 to10^{10}) grown under specified conditions were collected by centrifugation at
490 4,500g for 15 min at 4°C and resuspended in 7 ml ice-cold fresh 4% formaldehyde in 1× PBS. Fixation
491 was carried out overnight at 4°C with gentle shaking. Following fixation, cells were pelleted by

492 centrifugation at 4,500g for 15 min at 4°C and resuspended in 700 µl PBS-RI (1× PBS supplemented
493 with 0.1 U/ml NxGen RNase Inhibitor) in a nuclease-free 1.5 ml microcentrifuge tube (Axygen,
494 14324061). All subsequent centrifugations were performed at 12,700 rpm for 4 min at 4°C. Cells were
495 pelleted and resuspended in 700 µl PBS-RI, centrifuged again under the same conditions, and
496 resuspended in 350 µl PBS-RI. Then, 350 µl of 100% ethanol was added to the cell suspension and
497 mixed gently by pipetting. Immediately afterward, cells were washed twice with 700 µl PBS-RI. After the
498 second wash, cells were resuspended in 1 ml of ice-cold 100 mM Tris-HCl-RI (100 mM Tris-HCl pH 7.5
499 supplemented with 100 U/ml SUPERase-In RNase Inhibitor). Cells were diluted 1:100 in PBS and
500 counted using a hemocytometer (Bulldog-Bio, DHC-N420) to determine its concentration.

501 For each permeabilization reaction, up to 1×10^8 cells were resuspended in 250 µl of 0.04% Tween-20
502 in PBS-RI and incubated on ice for 3 min. Subsequently, 1 ml of ice-cold PBS-RI was added, and cells
503 were pelleted by centrifugation. The pellet was resuspended in 400 µl of lysozyme solution (100 mM
504 Tris-HCl pH 8.0, 50 mM EDTA, 250 U/ml SUPERase-In RNase Inhibitor, 2.5 mg/ml lysozyme) and
505 incubated at 37°C for 15 min. Following incubation, 1 ml of PBS-RI was added, cells were pelleted by
506 centrifugation and resuspended in 175 µl of PBS-RI. Cell concentration was determined using a
507 hemocytometer.

508 **In situ rRNA depletion and gDNA digestion**

509 Immediately following cell permeabilization, 4×10^7 cells were pelleted and resuspended in 11 µl of
510 nuclease-free water. The rRNA depletion was carried out using a thermostable RNase H-based
511 protocol with the NEBNext Bacterial rRNA Depletion Kit as described previously[23]. Specifically, 2 µl of
512 NEBNext rRNA Depletion Solution and 2 µl of Probe Hybridization Buffer were added to the cells on ice.
513 Hybridization was performed using the PCR cycler with following thermal profile (lid set to 55°C): 50°C
514 for 2 min, then ramped down to 22°C at 0.1°C/sec, followed by a 5-min hold at 22°C. Immediately after
515 hybridization, RNase H digestion was initiated by adding 2 µl of RNase H Reaction Buffer, 2 µl of

516 Thermostable RNase H, and 1 µl of nuclease-free water. The reaction was incubated at 50°C for 30 min
517 (lid at 55°C).

518 Following rRNA depletion, cells were centrifuged and resuspended in 10 µl of DNase-RI buffer (1 µl 10×
519 DNase I Reaction Buffer, 1 µl DNase I, 0.5 µl SUPERase-In RNase Inhibitor, and 7.5 µl nuclease-free
520 water). The mixture was incubated at room temperature for 30 min. To terminate DNase activity, 1 µl of
521 Stop Solution was added, followed by incubation at 50°C for 10 min. Afterward, cells were centrifuged
522 and washed twice with 100 µl of PBS-RI. The final cell pellet was resuspended in 20 µl of 0.5× PBS-RI
523 and used immediately for in-cell reverse transcription.

524 **Modifications to the previously published BacDrop protocol[23]**

525 To improve barcoding efficiency relative to the previously published BacDrop_V1 workflow, we
526 implemented a modified barcoding scheme in BacDrop_V2 that changes how round-2 barcodes (CB2)
527 are appended. In BacDrop_V1, in-cell reverse transcription (RT) is performed using RT primers
528 carrying the round-1 barcode (CB1), followed by in-cell 3′ poly(A) tailing of the newly synthesized
529 cDNA. Cells are then encapsulated into droplets, where oligo(dT)-primed second-strand synthesis
530 generates a cDNA duplex whose 5′ end can anneal to the 10x gel-bead oligonucleotide carrying a
531 unique barcode; polymerase extension subsequently copies the bead barcode onto the molecule to
532 introduce the round-2 barcode (CB2). In BacDrop_V2, we retained in-cell RT and CB1 incorporation but
533 redesigned the RT primer architecture (Supplementary Table 17) such that the cDNA produced in cells
534 is compatible with a ligation-based in-droplet cell barcoding (CB2). Following in-cell RT, we omitted the
535 in-cell poly(A) tailing step in BacDrop_V1 and proceeded directly to droplet encapsulation using the
536 same ATAC-seq kit from 10x Genomics. Within droplets, CB2 was introduced by a bridge-oligo-
537 mediated (Supplementary Table 18) ligation reaction that directly joins the cDNA (via the RT-primer
538 encoded 5′ end modified with a phosphate group) to the 10x ATAC-seq gel-bead oligonucleotide
539 containing the bead-specific barcode, thereby replacing the V1 polymerase-driven CB2 barcoding step

540 based on second-strand synthesis. This ligation-based round-2 barcoding strategy and primer/bridge-
541 oligo design principles were adapted from the published SciFi-RNA-seq and M3-seq protocols[24,42]. After
542 droplet barcoding, cDNA from all droplets was pooled and purified, poly(A) tailing was performed at the
543 pooled stage, and oligo(dT)-primed second-strand synthesis was carried out prior to downstream library
544 construction. Subsequent steps followed the BacDrop V1 workflow, including tagmentation to add
545 Illumina adapters and PCR amplification for sequencing-ready libraries. We validated the modified
546 workflow by comparing pseudo-bulk profiles derived from BacDrop V2 to matched bulk RNA-seq data
547 and observed high concordance, indicating that the updated barcoding strategy did not introduce
548 appreciable bias (Supplementary Fig. 1b,c). Detailed protocols and V2-specific modifications are
549 provided below.

550 **In-cell reverse transcription and round 1 barcoding**

551 The first round of cell barcoding and multiplexing was conducted via RT in 96-well plates. Compared to
552 previously described BacDrop protocol, we modified our RT primers to optimize the round 1 and round
553 2 barcoding efficiency. The modified RT primers (Supplementary Table 17) containing both a unique
554 molecular identifier (UMI) and a round 1 cell barcode (CB1) were custom-synthesized (Integrated DNA
555 Technologies) at 100 μM and diluted to 5 μM in a 96-well PCR plate (Axygen, PCR-96-HS-C). Each well
556 contained a RT primer containing distinct, well-specific CB1 sequences, ensuring that every well
557 corresponded to a unique CB1 barcode. A phosphate group was added the 5' of each RT primer for the
558 ligation step in round 2 barcoding. Each well of the RT plate was preloaded with 5 μl of a distinct primer
559 (5 μM). Cells previously depleted of rRNA and genomic DNA were diluted in 0.5× PBS-RI and added at
560 2 μl per well to the primer-containing plates. The cell-primer mix was incubated at 55°C for 5 min to
561 facilitate primer annealing, followed by immediate cooling on ice. An RT master mix consisting of 0.5 μl
562 DTT (100 mM), 0.5 μl dNTP mix (10 mM each), 0.5 μl SUPERase-In RNase inhibitor, 2 μl Maxima RT
563 buffer, and 0.5 μl Maxima H Minus reverse transcriptase was added to each well. Reverse transcription
564 was carried out in the PCR cycler under the following program (lid at 60°C): Initial incubation at 22°C

565 for 30 min and 50°C for 10 min, followed by three thermocycling rounds of 8°C for 12 s, 15°C for 45 s,
566 20°C for 45 s, 30°C for 30 s, 42°C for 2 min, 50°C for 3 min. The reaction ended with a final 5-min
567 incubation at 50°C and holding at 4°C. Following RT, cells were pelleted and washed 2 times with PBS-
568 RI, then resuspended in 20 µl nuclease-free water supplemented with 200 U/ml SUPERase-In RNase
569 inhibitor (H_2O-RI). Cell density was subsequently determined using a hemocytometer.

570 **Droplet generation**

571 The round 2 barcoding was modified from the previous described BacDrop_V1 protocol to increase the
572 coverage and barcoding efficiency. Specifically, we replaced the previous second strand synthesis
573 protocol with a thermo-ligation protocol as described in several other established scRNA-seq protocols .
574 For droplet formation, the Chromium Next GEM Chip H and the Single Cell ATAC Library & Gel Bead
575 Kit were utilized following the instructions with minor adjustments. Unused wells on the chip were filled
576 with 50% glycerol, specifically, 70 µl in row 1, 50 µl in row 2, and 40 µl in row 3. Cells prepared for
577 encapsulation were diluted with H_2O-RI to a final volume of 63 µl. Just before loading onto the chip, the
578 cell suspension was mixed with a ligation master mix consisting of 11.5 µl Ampligase buffer, 2.3 µl
579 100 µM bridge oligo (BOa, Supplementary Table 18), 2.3 µl Ampligase, and 1.5 µl Reducing Agent B
580 (Single Cell ATAC Library & Gel Bead Kit). A total of 70 µl of the resulting mixture was loaded into row 1
581 of the chip. 50 µl of gel beads embedded with round 2 barcodes (CB2) and 40 µl of partitioning oil were
582 loaded into rows 2 and 3 of the Chromium chip, respectively. The chip was then processed using the
583 Chromium iX controller, generating an emulsion of approximately 100 µl containing encapsulated single
584 cells.

585 **Round 2 barcode ligation**

586 Following droplet generation, the emulsion was evenly distributed into four individual PCR tubes
587 (approximately 25 µl per tube) using TempAssure 8-tube PCR strips (USA Scientific, 14024780). To
588 each tube, 25 µl of FC-40 oil was first added to the bottom, followed by 50 µl of mineral oil layered on
589 top of the emulsion, forming a biphasic mixture. Tubes were then subjected to ligation in a thermal

590 cycler using the following program (lid at 105°C): 12 cycles of 95°C for 30 s and 59°C for 2 min,
591 followed by hold at 15°C. After ligation, samples were left at room temperature for 15 min for better
592 phase separation. The upper mineral oil and lower FC-40 oil layers were carefully removed by pipetting,
593 ensuring the droplet-containing middle layer remained undisturbed.

594 **Breaking emulsions and cDNA purification**

595 All reagents required for breaking emulsions were sourced from the Single Cell ATAC Library & Gel
596 Bead Kit. To disrupt the emulsion in each PCR tube, 32 μl of Recovery Agent was added at room
597 temperature. Tubes were gently inverted ten times and briefly spun down to ensure complete phase
598 separation. The lower pink Recovery Agent and partitioning oil layer was carefully removed. cDNA
599 purification was initiated using Dynabeads MyOne SILANE. Specifically, for each sample, 45.5 μl
600 Cleanup Buffer, 2 μl Dynabeads, 1.25 μl Reducing Agent B, and 1.25 μl nuclease-free water were
601 added. After a 10-min incubation at room temperature with gentle mixing, tubes were placed on a
602 magnetic rack, and beads were washed twice using freshly prepared 80% ethanol. After the second
603 ethanol wash was removed, cDNA was eluted in 40 μl of a custom elution buffer (98 μl Buffer EB, 1 μl
604 10% Tween-20, and 1 μl Reducing Agent B). The eluate was transferred to a new PCR tube for further
605 purification using 1.25× SPRIselect beads, and the final cDNA was recovered in 43 μl nuclease-free
606 water.

607 **TdT tailing and second strand of cDNA synthesis**

608 Compared to the original BacDrop_V1 protocol, the terminal deoxynucleotidyl transferase (TdT) tailing
609 and second-strand synthesis steps were performed after cDNA purification from the second-round
610 droplet barcoding. In the modified workflow, TdT tailing was performed on purified cDNA rather than on
611 permeabilized cells. A total of 43 μl of barcoded cDNA (containing CB1 and CB2) was mixed with 5 μl of
612 10× TdT buffer, 1 μl of 100 mM dATP, and 1 μl of TdT enzyme (20 U/μl), resulting in a final reaction
613 volume of 50 μl. The reaction was incubated at 37°C for 30 min. To terminate the reaction, 10 μl of
614 0.2 M EDTA (pH 8.0) was added, followed by a 10-min incubation at room temperature. The reaction

615 mixture was then purified using a 2× SPRIselect bead cleanup and eluted in 44 µl of nuclease-free
616 water.

617 Second-strand cDNA synthesis was carried out using the KAPA HiFi HotStart ReadyMix. Each 100 µl
618 reaction included 44 µl of purified single-stranded cDNA, 50 µl of 2× KAPA HiFi HotStart ReadyMix, 3 µl
619 of 10 µM SMRT_dT primer, and 3 µl of 10 µM P5 primer. The PCR cycling protocol was as follows (lid at
620 105°C): 95°C for 30 s; 39°C for 5 min; four cycles of 65°C for 10 min, 98°C for 20 s, 62°C for 15 s, and
621 72°C for 2 min; followed by 72°C for 5 min and a final hold at 10°C. The amplified product was then
622 purified using a 2× SPRIselect bead cleanup and eluted in 50 µl of nuclease-free water. To assess
623 cDNA concentration, 2 µl of each sample was measured using a Qubit fluorometer with the Qubit 1×
624 dsDNA High Sensitivity (HS) Assay Kit. Samples yielding decent DNA concentration were selected for
625 downstream library construction.

626 **Enrichment of cDNA**

627 Prior to cDNA amplification, a quantitative PCR (qPCR) assay was performed to determine the optimal
628 number of enrichment cycles. The reaction consisted of 1 µl cDNA template, 5 µl KAPA HiFi HotStart
629 ReadyMix, 0.3 µl each of P5 (10 µM) and SMRT_PCR primers (10 µM) (Supplementary Table 18), 2 µl
630 of 5× SYBR Green dye, and 1.4 µl nuclease-free water. qPCR was run on a real-time thermal cycler
631 (CFX Duet, BioRad) using the following cycling conditions: initial denaturation at 98°C for 2 min; 30
632 cycles of 98°C for 20 s, 67°C for 20 s, and 72°C for 3 min; followed by a final extension at 72°C for 5
633 min and hold at 4°C. The cycle threshold (Ct) corresponding to the early exponential phase of
634 amplification was used to guide subsequent cDNA enrichment. For large-scale amplification, 44 µl of
635 cDNA was combined with 50 µl of 2× KAPA HiFi HotStart ReadyMix, 3 µl each of P5 and SMRT_PCR
636 primers (10 µM) to a total volume of 100 µl. The PCR was performed using the same thermal cycling
637 program as in the qPCR, applying the Ct-derived cycle number. Following amplification, the product
638 was cleaned up using a 0.6× SPRIselect bead purification protocol and eluted in 30 µl of nuclease-free

639 water for subsequent sequencing library preparation. cDNA concentration was quantified using a Qubit
640 fluorometer in combination with the Qubit 1× dsDNA High Sensitivity (HS) Assay Kit.

641 **Illumina library preparation for sequencing**

642 Sequencing libraries were prepared using the Illumina Nextera XT DNA Library Prep Kit with protocol
643 adjustments. For each 20 µl tagmentation reaction, 1 to 2 ng of enriched cDNA was mixed with 5 µl of
644 Amplicon Tagment Mix (ATM) and 10 µl of Tagment DNA Buffer (TD). The mixture was incubated at
645 55°C for 5 min in a thermocycler, followed by a hold at 10°C. Once the reaction reached 10°C, 5 µl of
646 Neutralize Tagment Buffer (NT) was added immediately. The solution was mixed by pipetting up and
647 down 10 times and incubated at room temperature for 5 min before proceeding to PCR amplification.
648 Next, 5 µl of P5 primer (5 µM) (Supplementary Table 18), 5 µl of Index 1 primer (N7**) (FC-131-2001,
649 Illumina), and 15 µl of Nextera PCR Master Mix (NPM) were added to the 25 µl tagmented mixture to
650 form a 50 µl PCR reaction. The thermal cycling program included an initial extension at 72°C for 3 min
651 and denaturation at 95°C for 30 s, followed by 5 cycles of 95°C for 10 s, 55°C for 30 s, and 72°C for 30
652 s, and a final extension at 72°C for 5 min. The PCR tubes were immediately placed on ice to avoid
653 over-amplification.

654 To determine the optimal number of additional amplification cycles, a qPCR assay was set up using 5 µl
655 of the partially amplified library, 3 µl of NPM, 1 µl each of P5 and Index 1 primers (5 µM), 3 µl of 5×
656 SYBR Green, and 2 µl of nuclease-free water. The qPCR was performed under the same cycling
657 conditions. The cycle number corresponding to the midpoint of the exponential amplification curve was
658 selected for the remaining library amplification. The remaining 45 µl of the initial PCR mixture was
659 subjected to additional amplification using the cycle count determined by qPCR. Final libraries were
660 purified with a 1× SPRIselect bead cleanup and eluted in 25 µl of nuclease-free water. Library
661 concentrations were quantified using the Qubit 1× dsDNA High Sensitivity (HS) Assay Kit and a Qubit
662 fluorometer.

663 **Illumina sequencing of the BacDrop_V2 library**

664 Prepared libraries were diluted to the appropriate concentrations and sequenced on the Illumina
665 NovaSeq X plus platform using standard Illumina sequencing primers. Sequencing was performed with
666 the following read configuration: Read 1: 60 bp, Read 2: 40 bp, Index 1: 8 bp, and Index 2: 30 bp.

667 **Antibiotic killing curve assay**

668 To investigate antibiotic persistence across growth phases, bacterial cultures were grown in MHB to
669 stationary, lag, or exponential phase as described above. A lethal final concentration of either
670 meropenem (2 μg/ml) or ciprofloxacin (2.5 μg/ml) was added to the culture and incubate at 37°C with
671 shaking. At the specified time points post-treatment, 1 ml of culture was harvested, centrifuged (12,700
672 rpm, 3 min), resuspended in 100 μl PBS, and subsequently serially diluted in PBS. Ten microliters of
673 each were spotted onto LB agar plates. After incubation at 37°C for 16-18 hours, colony-forming units
674 (CFUs) were counted to quantify survived bacteria. Survival rates were calculated by normalizing CFUs
675 at each time point to the initial CFUs at time zero (before antibiotic exposure). Each killing assay was
676 performed with at least three biological replicates.

677 **Construction of GFP reporter strains**

678 GFP reporter plasmids were constructed by inserting the target promoter into the pUA139[43] vector
679 upstream of the *gfp* reporter gene. Briefly, the plasmid backbone was amplified by PCR using Q5 High-
680 Fidelity 2× Master Mix with primers PMSJ060 and PMSJ061 (Supplementary Table 18). Synthesized
681 promoter of *lpp1*, *osmB*, *rpoS*, *recA*, *dnaK*, and *fusA* genes (Supplementary Table 18), each containing
682 homologous overlaps with the plasmid backbone, were assembled with the amplified pUC139 fragment
683 using the NEBuilder HiFi DNA Assembly Cloning Kit. The assembled constructs were transformed into
684 NEB 10-beta for propagation. Plasmid integrity and sequence correctness were verified via whole
685 plasmid sequencing. The validated reporter plasmids (Supplementary Table 15), pUA139_P*lpp1_gfp*,
686 pUA139_P*osmB_gfp*, pUA139_P*rpoS_gfp*, pUA139_P*recA_gfp*, and pUA139_P*dnaK_gfp*, were
687 subsequently transformed into *K. pneumoniae* MGH66 WT by electroporation as previously described .
688 This yielded the reporter strains (MGH66:pUA139_P*lpp1_gfp*, MGH66:pUA139_P*osmB_gfp*,

689 MGH66:pUA139_P*rpoS_gfp*, MGH66:pUA139_P*recA_gfp*, and MGH66:pUA139_P*dnaK_gfp*) for flow
690 cytometric sorting and analysis.

691 **Flow cytometry analysis and cell sorting for antibiotic killing assay**

692 Exponential-phase cultures of reporter strains were prepared as described above in MHB medium
693 supplied with 50 μg/ml kanamycin (Sigma-Aldrich, K1377) to maintain the reporter plasmid. Upon
694 reaching exponential phase, the reporter strains *K. pneumoniae* MGH66: P*osmB:gfp*, MGH66:
695 P*rpoS:gfp*, and MGH66: P*fusA:gfp* were treated with 2 μg/ml meropenem for 10 min. Following
696 antibiotic exposure, cells were diluted in PBS staining buffer (PBS containing DAPI) to a final
697 concentration of 10^6 cells/ml, and immediately analyzed by flow cytometry. For persister assay under
698 the treatment of meropenem, GFP-low and GFP-high subpopulations were isolated by fluorescence-
699 activated cell sorting (FACS). From each sorted population, approximately 10^6 cells were collected into
700 2 ml MHB medium or MHB medium supplemented with 2 μg/ml meropenem. From the antibiotic-free
701 MHB medium, a 50 μl aliquot of sorted cells was immediately serially diluted and plated on LB agar to
702 determine the initial CFUs. The cells sorted into MHB medium containing meropenem were incubated
703 at 37°C with shaking for 4 hours, washed, serially diluted in PBS, and plated on LB agar. CFUs were
704 enumerated to quantify surviving bacteria. Three biological replicates were performed in each
705 experiment.

706 For flow cytometry analysis of stationary-phase cells exposed to antibiotics, *K. pneumoniae* MGH66
707 carrying the reporter plasmids pUA139_P*lpp1_gfp* or pUA139_P*recA_gfp* was cultured to stationary
708 phase in MHB supplemented with kanamycin (50 μg/ml), as described above. Stationary-phase
709 MGH66:pUA139_P*lpp1_gfp* and MGH66:pUA139_P*recA_gfp* cells were exposed to meropenem (2
710 μg/ml) or ciprofloxacin (2.5 μg/ml), respectively, for 30 min. Following treatment, cells were washed,
711 resuspended in PBS, and immediately analyzed by flow cytometry. Three biological replicates were
712 performed in each experiment.

713 **Heat shock and killing assay**

714 Cells at the exponential growth phase were harvested and subjected to heat shock by incubation at
715 42°C for 30 min. Immediately following heat treatment, the cultures were exposed to a lethal dose of
716 meropenem (2 μg/ml) and incubated for 4 hours at 37°C. Surviving cells were quantified by serial
717 dilution and plating on LB agar plates, followed by colony enumeration after overnight incubation. The
718 killing assay after heat shock was performed with three biological replicates.

719 **Construction of *K. pneumoniae rpoS* gene deletion mutant**

720 The *rpoS* gene knockout strain was generated via homologous recombination using the temperature-
721 sensitive plasmid pKOV[44]. Genomic DNA from overnight cultures of the MGH66 WT strain was
722 extracted using the Quick-DNA HMW MagBead Kit. DNA fragments (~1 kb each) flanking the *rpoS*
723 gene were amplified from MGH66 genomic DNA by PCR with Q5 High-Fidelity 2× Master Mix using
724 primer pairs PMSJ087/PMSJ088 and PMSJ089/PMSJ090 (Supplementary Table 18). The pKOV
725 plasmid backbone was similarly amplified using primers PMSJ064 and PMSJ065 (Supplementary Table
726 18). The three PCR products were assembled via NEBuilder HiFi DNA Assembly based on designed
727 overlapping regions to generate the recombinant plasmid pKOV_up_down_*rpoS*. The resulting
728 construct was transformed into *E. coli* NEB 10-beta and propagated at 30°C on LB agar supplemented
729 with 25 μg/ml chloramphenicol (Sigma-Aldrich, C0378). Plasmid integrity was verified through whole-
730 plasmid sequencing.

731 The confirmed pKOV_up_down_*rpoS* plasmid was introduced into *K. pneumoniae* MGH66 WT via
732 electroporation. Transformants were selected on LB agar supplemented with 25 μg/ml chloramphenicol
733 at 37°C. Owing to the temperature-sensitive origin of replication in pKOV, plasmid integration into the
734 chromosome, via single-crossover recombination at either the upstream or downstream homology arm,
735 was induced by shifting the incubation temperature to 42°C. To facilitate resolution of the integrated
736 plasmid and achieve double-crossover recombination, integrant strains were cultured in LB without
737 antibiotics at 37°C. Cultures were then diluted and plated onto LB agar without antibiotic. Individual
738 colonies were screened for chloramphenicol sensitivity to identify clones that had lost the plasmid

739 backbone. PCR screening using primers PMSJ087/PMSJ090 was performed to confirm deletion of the
740 *rpoS* gene. The final *rpoS* depletion mutant strain MGH66:Δ*rpoS* was validated by whole-genome
741 sequencing.

742 **Nutrient shift for killing assay**

743 To investigate how nutrient shifts affect antibiotic persistence in stationary-phase *K. pneumoniae*,
744 overnight cultures of the MGH66 WT strain were prepared by inoculating glycerol stocks into 80 ml of
745 MHB in 500 ml flasks and incubating at 37°C with shaking. The following day, 1 ml of the culture was
746 set aside, and the remaining volume was centrifuged at 4,500× g for 15 min. The supernatant was
747 filtered using a 0.22 μm PES membrane (Millipore Express PLUS, S2GPU02RE) to obtain spent
748 medium. The reserved overnight culture was diluted 1:100 into the spent medium. Aliquots of 1 ml were
749 dispensed into 1.5 ml tubes and individually supplemented with either no additive or one of the following
750 nutrients: 20 mM of glucose (Sigma-Aldrich, G8270), 10 mM of ammonium sulfate (Sigma-Aldrich,
751 A4915), 10 mM of glutamine (Sigma-Aldrich, 1294808), 1% of casamino acids (Sigma-Aldrich, 65072-
752 00-6), 2 mM of magnesium sulfate (Sigma-Aldrich, M2643), 10 mM Ammonium iron (II) sulfate
753 hexahydrate (Sigma-Aldrich, 09719, simplified as $FeSO_4$). Cultures were then treated with meropenem
754 (2 μg/ml) or ciprofloxacin (2.5 μg/ml) and incubated at 37°C with shaking. After 4 hours of antibiotic
755 exposure, cells were harvested by centrifugation, resuspended in 100 μl PBS, serially diluted, and
756 plated on LB agar plate. Surviving cells were quantified by colony counting following overnight
757 incubation. All experiments were performed in triplicate.

758 **Thiourea reverses Fe^{2+}-enhanced ciprofloxacin killing assay**

759 Stationary-phase *K. pneumoniae* MGH66 cells were diluted 1:100 into 1 ml spent medium in 1.5 ml
760 tubes and supplemented with one of the following conditions: no additive, ciprofloxacin alone (2.5
761 μg/ml), $FeSO_4$ alone (10 mM), thiourea alone (200 mM, Sigma-Aldrich, T8656), $FeSO_4$ plus
762 ciprofloxacin, $FeSO_4$ plus thiourea, or $FeSO_4$ with both ciprofloxacin and thiourea. Cultures were
763 incubated at 37°C with shaking for 4 hours, then harvested by centrifugation, washed, serially diluted in

764 PBS, and plated on LB agar. CFUs were enumerated after overnight incubation to quantify surviving
765 cells. All conditions were performed in triplicate.

766 **Bulk RNA-seq**

767 Stationary-phase *K. pneumoniae* MGH66 cells were diluted 1:100 into 1 ml of spent medium in 1.5 ml
768 tubes and supplemented with either no additive, $FeSO_4$ alone (10 mM), or $FeSO_4$ combined with
769 ciprofloxacin (2.5 µg/ml). Cultures were incubated at 37°C with shaking for 4 hours, after which cells
770 were harvested by centrifugation and resuspended in 500 µl TRIzol (Invitrogen, 15596026) for total
771 RNA extraction. RNA was purified using the Direct-zol RNA Miniprep Kit (Zymo, R2052) according to
772 the supplied protocol. For library preparation, 100 ng of total RNA was used with the NEBNext Ultra II
773 Directional RNA Library Prep Kit (NEB, E7760S). Sequencing was performed in paired-end mode on an
774 Illumina NextSeq2000 platform.

775 **Computational analysis**

776 **Processing of raw sequencing data**

777 Raw sequencing reads were trimmed and quality-checked using *fastp* (v0.19.6)[45]. Demultiplexing was
778 performed based on CB1 with a custom shell script to separate samples. Cell barcodes and UMI
779 sequences were extracted from the reads and incorporated into read headers using *UMI-tools*
780 (v1.1.4)[46]. Processed reads were then aligned to the *Klebsiella pneumoniae* MGH 66 strain genome
781 (BioProject: PRJNA1309751) using *BWA* (v0.7.17)[47]. Gene-level quantification was performed with
782 *featureCounts* (v2.0.5)[48], and the final count table was generated with *UMI-tools*.

783 **Analysis of BacDrop_v2 data**

784 For each scRNA-seq experiment using BacDrop_V2, approximately 100,000 cells were barcoded per
785 sample, and sequencing was performed at a depth of ~2,000–3,000 reads per cell. For downstream
786 analysis, the top 10,000 cells with the highest UMI counts were selected for each sample, consistent
787 with the published BacDrop data analysis pipeline[23], which prioritizes cells with sufficient transcript

788 coverage for robust state identification in bacterial scRNA-seq. Count tables were analyzed using the
789 *Seurat* package (v5.1.0)[49]. Quality control was performed by filtering out low-quality cells with fewer
790 than 15 detected genes, as well as potential barcode collisions represented by cells with more than 300
791 detected genes. Gene counts were normalized using default *Seurat* parameters, and the top 2,000
792 variable features were identified with the variance-stabilizing transformation (vst) method. All genes
793 were then scaled across cells, and dimensionality reduction and clustering were performed by principal
794 component analysis (PCA) on the variable features, followed by UMAP. Marker genes for each cluster
795 were identified with *FindAllMarkers* using a $\log_2$ fold change threshold of 0.5. Cell states were
796 annotated by GO and pathway enrichment analysis of cluster marker genes ($\log_2$ fold change > 1,
797 adjusted $p < 0.05$) using STRING (v12.0)[50].

798 **Bulk RNA-seq analysis**

799 To assess potential bias during single-cell RNA library construction, we performed correlation analysis
800 between bulk RNA-seq and scRNA-seq data. Cell barcode and UMI sequences were removed from
801 scRNA-seq reads using *fastp* (v0.24.0). These trimmed reads, together with bulk RNA-seq reads, were
802 aligned to the reference genome with *BWA* (v0.7.19). Read counts were quantified using *featureCounts*
803 (v2.1.1) to generate a raw gene count matrix, and gene-level correlations were visualized with
804 *Matplotlib Pyplot*.

805 For bulk RNA-seq differential expression analysis, raw sequencing reads were quality-checked with
806 *fastp* (v0.24.0) and aligned to the reference genome using *BWA* (v0.7.19). Gene-level expression
807 matrices were generated with *featureCounts* (v2.1.1), and raw counts were normalized with the *rlog*
808 function in the *DESeq2* package (v1.46.0)[51]. Normalized expression data were visualized with the
809 *ComplexHeatmap* package. Differentially expressed genes were identified using *DESeq2*, with adjusted
810 p values and fold changes calculated. Volcano plots were generated with *ggplot2*.

811 **References**

1 Elowitz, M. B., Levine, A. J., Siggia, E. D. & Swain, P. S. Stochastic gene expression in a single cell. *Science* **297**, 1183-1186 (2002). https://doi.org:10.1126/science.1070919

2 Spudich, J. L. & Koshland, D. E., Jr. Non-genetic individuality: chance in the single cell. *Nature* **262**, 467-471 (1976). https://doi.org:10.1038/262467a0

3 Veening, J. W., Smits, W. K. & Kuipers, O. P. Bistability, epigenetics, and bet-hedging in bacteria. *Annu Rev Microbiol* **62**, 193-210 (2008). https://doi.org:10.1146/annurev.micro.62.081307.163002

4 Ackermann, M. A functional perspective on phenotypic heterogeneity in microorganisms. *Nat Rev Microbiol* **13**, 497-508 (2015). https://doi.org:10.1038/nrmicro3491

5 Bakkeren, E., Diard, M. & Hardt, W. D. Evolutionary causes and consequences of bacterial antibiotic persistence. *Nat Rev Microbiol* **18**, 479-490 (2020). https://doi.org:10.1038/s41579-020-0378-z

6 Balaban, N. Q., Merrin, J., Chait, R., Kowalik, L. & Leibler, S. Bacterial persistence as a phenotypic switch. *Science* **305**, 1622-1625 (2004). https://doi.org:10.1126/science.1099390

7 Dewachter, L., Fauvart, M. & Michiels, J. Bacterial Heterogeneity and Antibiotic Survival: Understanding and Combatting Persistence and Heteroresistance. *Mol Cell* **76**, 255-267 (2019). https://doi.org:10.1016/j.molcel.2019.09.028

8 Windels, E. M. *et al.* Bacterial persistence promotes the evolution of antibiotic resistance by increasing survival and mutation rates. *ISME J* **13**, 1239-1251 (2019). https://doi.org:10.1038/s41396-019-0344-9

9 Balaban, N. Q. *et al.* Definitions and guidelines for research on antibiotic persistence. *Nat Rev Microbiol* **17**, 441-448 (2019). https://doi.org:10.1038/s41579-019-0196-3

10 Lewis, K. Persister cells. *Annu Rev Microbiol* **64**, 357-372 (2010). https://doi.org:10.1146/annurev.micro.112408.134306

11 Goormaghtigh, F. *et al.* Reassessing the Role of Type II Toxin-Antitoxin Systems in Formation of Escherichia coli Type II Persister Cells. *mBio* **9** (2018). https://doi.org:10.1128/mBio.00640-18

12 Harms, A., Maisonneuve, E. & Gerdes, K. Mechanisms of bacterial persistence during stress and antibiotic exposure. *Science* **354** (2016). https://doi.org:10.1126/science.aaf4268

13 Battesti, A., Majdalani, N. & Gottesman, S. The RpoS-mediated general stress response in Escherichia coli. *Annu Rev Microbiol* **65**, 189-213 (2011). https://doi.org:10.1146/annurev-micro-090110-102946

14 Dorr, T., Vulic, M. & Lewis, K. Ciprofloxacin causes persister formation by inducing the TisB toxin in Escherichia coli. *PLoS Biol* **8**, e1000317 (2010). https://doi.org:10.1371/journal.pbio.1000317

15 Fung, D. K. *et al.* A shared alarmone-GTP switch controls persister formation in bacteria. *Nat Microbiol* **10**, 1617-1629 (2025). https://doi.org:10.1038/s41564-025-02015-6

16 Hong, S. H., Wang, X., O'Connor, H. F., Benedik, M. J. & Wood, T. K. Bacterial persistence increases as environmental fitness decreases. *Microb Biotechnol* **5**, 509-522 (2012). https://doi.org:10.1111/j.1751-7915.2011.00327.x

17 Nguyen, D. *et al.* Active starvation responses mediate antibiotic tolerance in biofilms and nutrient-limited bacteria. *Science* **334**, 982-986 (2011). https://doi.org:10.1126/science.1211037

18 Murakami, K. *et al.* Role for rpoS gene of Pseudomonas aeruginosa in antibiotic tolerance. *FEMS Microbiol Lett* **242**, 161-167 (2005). https://doi.org:10.1016/j.femsle.2004.11.005

19 Zhai, Y. *et al.* ppGpp and RNA-polymerase backtracking guide antibiotic-induced mutable gambler cells. *Mol Cell* **83**, 1298-1310 e1294 (2023). https://doi.org:10.1016/j.molcel.2023.03.003

20 Davis, K. M. & Isberg, R. R. Defining heterogeneity within bacterial populations via single cell approaches. *Bioessays* **38**, 782-790 (2016). https://doi.org:10.1002/bies.201500121

21 Blattman, S. B., Jiang, W., Oikonomou, P. & Tavazoie, S. Prokaryotic single-cell RNA sequencing by in situ combinatorial indexing. *Nat Microbiol* **5**, 1192-1201 (2020). https://doi.org:10.1038/s41564-020-0729-6

22 Kuchina, A. *et al.* Microbial single-cell RNA sequencing by split-pool barcoding. *Science* **371** (2021). https://doi.org:10.1126/science.aba5257
23 Ma, P. *et al.* Bacterial droplet-based single-cell RNA-seq reveals antibiotic-associated heterogeneous cellular states. *Cell* **186**, 877-891 e814 (2023). https://doi.org:10.1016/j.cell.2023.01.002
24 Wang, B. *et al.* Single-cell massively-parallel multiplexed microbial sequencing (M3-seq) identifies rare bacterial populations and profiles phage infection. *Nat Microbiol* **8**, 1846-1862 (2023). https://doi.org:10.1038/s41564-023-01462-3
25 Xu, Z. *et al.* Droplet-based high-throughput single microbe RNA sequencing by smRandom-seq. *Nat Commun* **14**, 5130 (2023). https://doi.org:10.1038/s41467-023-40137-9
26 Imdahl, F., Vafadarnejad, E., Homberger, C., Saliba, A. E. & Vogel, J. Single-cell RNA-sequencing reports growth-condition-specific global transcriptomes of individual bacteria. *Nat Microbiol* **5**, 1202-1206 (2020). https://doi.org:10.1038/s41564-020-0774-1
27 Blattman, S. B. *et al.* Identification and genetic dissection of convergent persister cell states. *Nature* **636**, 438-446 (2024). https://doi.org:10.1038/s41586-024-08124-2
28 Niu, H., Gu, J. & Zhang, Y. Bacterial persisters: molecular mechanisms and therapeutic development. *Signal Transduct Target Ther* **9**, 174 (2024). https://doi.org:10.1038/s41392-024-01866-5
29 Umetani, M. *et al.* Observation of persister cell histories reveals diverse modes of survival in antibiotic persistence. *Elife* **14** (2025). https://doi.org:10.7554/eLife.79517
30 Navon-Venezia, S., Kondratyeva, K. & Carattoli, A. Klebsiella pneumoniae: a major worldwide source and shuttle for antibiotic resistance. *FEMS Microbiol Rev* **41**, 252-275 (2017). https://doi.org:10.1093/femsre/fux013
31 Braun, V. & Rehn, K. Chemical characterization, spatial distribution and function of a lipoprotein (murein-lipoprotein) of the E. coli cell wall. The specific effect of trypsin on the membrane structure. *Eur J Biochem* **10**, 426-438 (1969). https://doi.org:10.1111/j.1432-1033.1969.tb00707.x
32 Drlica, K., Malik, M., Kerns, R. J. & Zhao, X. Quinolone-mediated bacterial death. *Antimicrob Agents Chemother* **52**, 385-392 (2008). https://doi.org:10.1128/AAC.01617-06
33 Dong, T., Kirchhof, M. G. & Schellhorn, H. E. RpoS regulation of gene expression during exponential growth of Escherichia coli K12. *Mol Genet Genomics* **279**, 267-277 (2008). https://doi.org:10.1007/s00438-007-0311-4
34 Metaane, S. *et al.* The stress sigma factor sigmaS/RpoS counteracts Fur repression of genes involved in iron and manganese metabolism and modulates the ionome of Salmonella enterica serovar Typhimurium. *PLoS One* **17**, e0265511 (2022). https://doi.org:10.1371/journal.pone.0265511
35 Allison, K. R., Brynildsen, M. P. & Collins, J. J. Metabolite-enabled eradication of bacterial persisters by aminoglycosides. *Nature* **473**, 216-220 (2011). https://doi.org:10.1038/nature10069
36 Basan, M. *et al.* Overflow metabolism in Escherichia coli results from efficient proteome allocation. *Nature* **528**, 99-104 (2015). https://doi.org:10.1038/nature15765
37 Li, Z., Nees, M., Bettenbrock, K. & Rinas, U. Is energy excess the initial trigger of carbon overflow metabolism? Transcriptional network response of carbon-limited Escherichia coli to transient carbon excess. *Microb Cell Fact* **21**, 67 (2022). https://doi.org:10.1186/s12934-022-01787-4
38 Touati, D. Iron and oxidative stress in bacteria. *Arch Biochem Biophys* **373**, 1-6 (2000). https://doi.org:10.1006/abbi.1999.1518
39 Wagner, D. E. & Klein, A. M. Lineage tracing meets single-cell omics: opportunities and challenges. *Nat Rev Genet* **21**, 410-427 (2020). https://doi.org:10.1038/s41576-020-0223-2
40 Ma, P. *et al.* Genetic determinants facilitating the evolution of resistance to carbapenem antibiotics. *Elife* **10** (2021). https://doi.org:10.7554/eLife.67310

41 Baba, T. *et al.* Construction of Escherichia coli K-12 in-frame, single-gene knockout mutants: the Keio collection. *Mol Syst Biol* **2**, 2006 0008 (2006). https://doi.org:10.1038/msb4100050

42 Datlinger, P. *et al.* Ultra-high-throughput single-cell RNA sequencing and perturbation screening with combinatorial fluidic indexing. *Nat Methods* **18**, 635-642 (2021). https://doi.org:10.1038/s41592-021-01153-z

43 Zaslaver, A. *et al.* A comprehensive library of fluorescent transcriptional reporters for Escherichia coli. *Nat Methods* **3**, 623-628 (2006). https://doi.org:10.1038/nmeth895

44 Link, A. J., Phillips, D. & Church, G. M. Methods for generating precise deletions and insertions in the genome of wild-type Escherichia coli: application to open reading frame characterization. *J Bacteriol* **179**, 6228-6237 (1997). https://doi.org:10.1128/jb.179.20.6228-6237.1997

45 Chen, S., Zhou, Y., Chen, Y. & Gu, J. fastp: an ultra-fast all-in-one FASTQ preprocessor. *Bioinformatics* **34**, i884-i890 (2018).

46 Smith, T., Heger, A. & Sudbery, I. UMI-tools: modeling sequencing errors in Unique Molecular Identifiers to improve quantification accuracy. *Genome research* **27**, 491-499 (2017).

47 Li, H. Aligning sequence reads, clone sequences and assembly contigs with BWA-MEM. *arXiv preprint arXiv:1303.3997* (2013).

48 Liao, Y., Smyth, G. K. & Shi, W. featureCounts: an efficient general purpose program for assigning sequence reads to genomic features. *Bioinformatics* **30**, 923-930 (2014).

49 Stuart, T. *et al.* Comprehensive integration of single-cell data. *cell* **177**, 1888-1902. e1821 (2019).

50 von Mering, C. *et al.* STRING: known and predicted protein-protein associations, integrated and transferred across organisms. *Nucleic Acids Res* **33**, D433-437 (2005). https://doi.org:10.1093/nar/gki005

51 Love, M. I., Huber, W. & Anders, S. Moderated estimation of fold change and dispersion for RNA-seq data with DESeq2. *Genome biology* **15**, 550 (2014).

Acknowledgements

We thank Drs. Elaine Tuomanen, Richard Lee, David Rogers, Jinna Bai for comments on the manuscript. We thank the Hartwell Center at St. Jude Children's Research Hospital for sequencing, and the flow core for flow cytometry analysis. This research is funded by National Institute of General Medical Sciences grant R35GM157243 to P.M. and Children's Infection Defense Center at St. Jude Children's Research Hospital (PROJ-1001461) to P.M.

Author contributions

Q.L., X.L. and P.M. conceived the study and performed the experiments. Q.L., Z.Y., A.I., T.S., J.W.R. and P.M. developed the methodology. Q.L., Z.Y. and P.M. performed data analysis and visualization.

Q.L., Z.Y. and P.M. wrote the manuscript draft. Q.L., Z.Y., J.W.R. and P.M. revised and edited the manuscript. J.W.R. and P.M. supervised the study. P.M. provided the funding and resource.

Competing interests

Authors declare that they have no competing interests.

Materials & Correspondence

The bacterial strains and constructs will be available upon request to P.M. after the publication of this manuscript.

Statistical information

All statistical analyses were carried out using GraphPad Prism 10. One-way ANOVA was applied to compare means across multiple groups, while unpaired *t*-tests were used for comparisons between two independent groups. Sample sizes, statistical tests, and measures of precision are reported in the figure legends and results sections.

Supplementary Information

Supplementary Figures 1 to 17

Supplementary Tables 1 to 18

Data Availability

The processed counting matrix of all scRNA-seq experiments have been deposited to GEO repository (GEO: GSE306416). The raw sequencing data of bulk RNA-seq and scRNA-seq experiments have been deposited to SRA depository (PRJNA1310171). All data will be publicly available upon the publication of this manuscript. All scRNA and bulk RNA analysis scripts are deposited at https://github.com/Zehui-stjude/BacDrop_v2 and will be publicly available upon the publication of this manuscript.

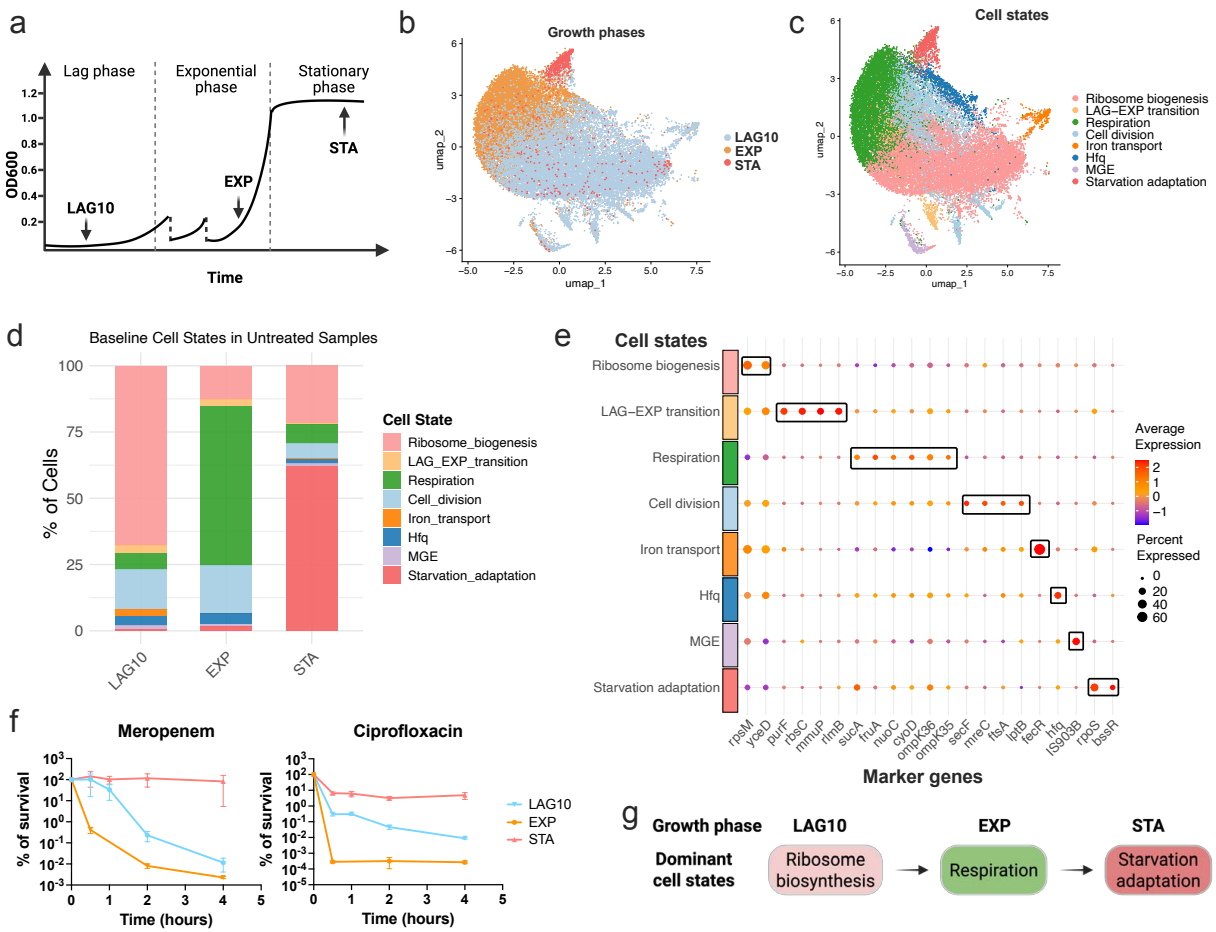

Figure 1. Growth-phase-specific transcriptional cell states underlie antibiotic persistence.

a, Schematic of the sampling strategy for scRNA-seq across three growth phases: early lag (10 minutes post-transfer to fresh medium, LAG10), exponential (EXP), and stationary phases (STA) under unperturbed conditions.

b, UMAP projection of single-cell transcriptomes from LAG10, EXP, and STA samples, colored by growth phase. Two independent biological replicates (n = 2) were included for each condition.

c, UMAP embedding colored by eight annotated cell states, identified based on gene expression markers across all growth phases.

d, Distribution of cell states across growth phases. Cell state proportions were averaged from two biological replicates.

e, Selected marker genes representative of each annotated cell state.

f, Killing dynamics of *K. pneumoniae* MGH66 following treatment with meropenem (2 μg/ml) or ciprofloxacin (2.5 μg/ml), initiated at different growth phases. Persistence levels differed by growth phase. CFU was quantified over time; data represent three independent biological replicates (n = 3), and error bars denote standard deviation.

g, Summary of growth-phase-dominated cell states.

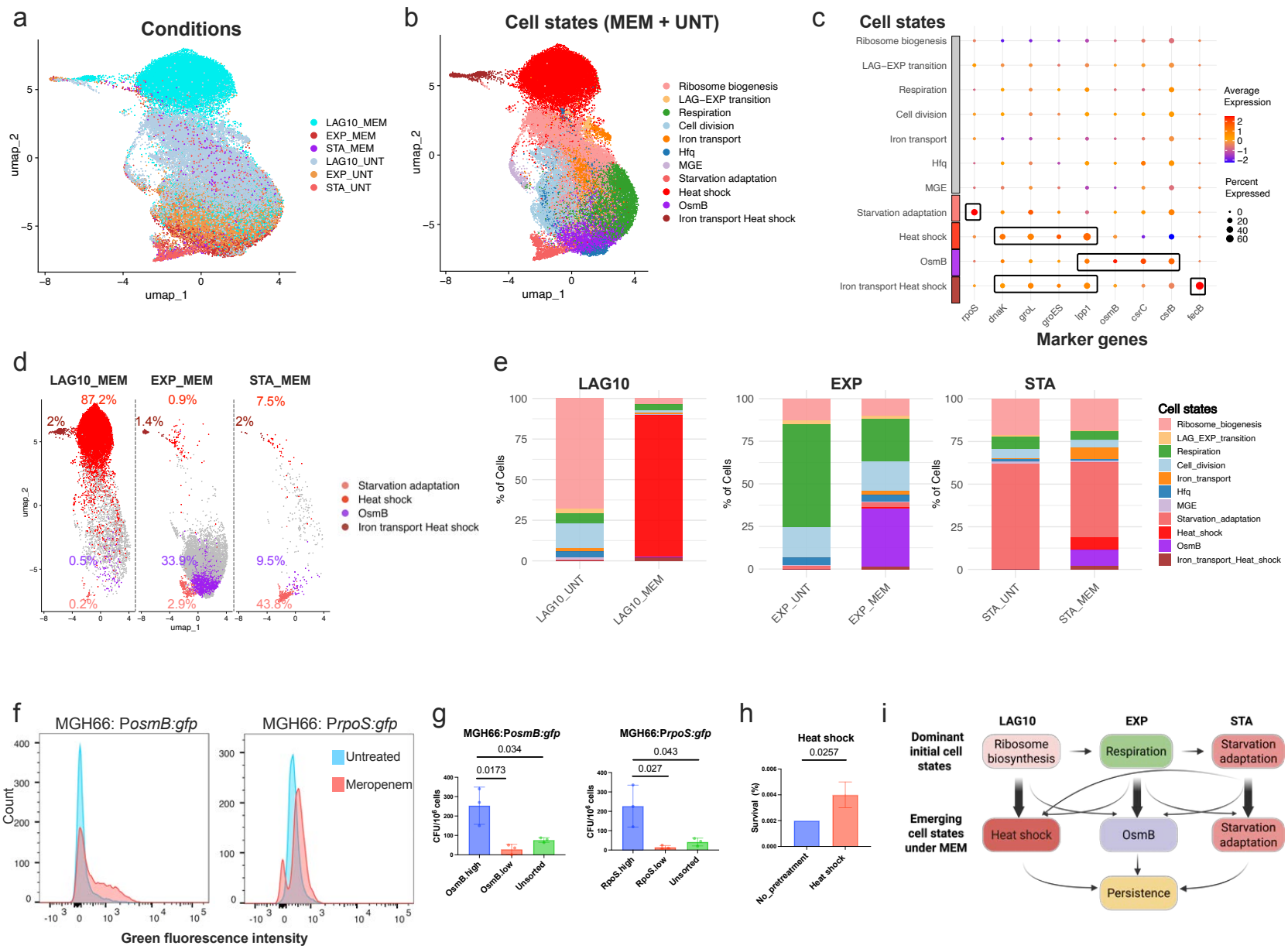
a
Conditions
umap_2
umap_1
LAG10_MEM
EXP_MEM
STA_MEM
LAG10_UNT
EXP_UNT
STA_UNT
b
Cell states (MEM + UNT)
Ribosome biogenesis
LAG−EXP transition
Respiration
Cell division
Iron transport
Hfq
MGE
Starvation adaptation
Heat shock
OsmB
Iron transport Heat shock
c
Cell states
Average Expression
Percent Expressed
rpoS
dnaK
groL
groES
lpp1
osmB
csrC
csiB
feoB
Marker genes
d
LAG10_MEM
EXP_MEM
STA_MEM
87.2%
2%
0.5%
0.2%
0.9%
1.4%
33.9%
2.9%
7.5%
2%
9.5%
43.8%
e
LAG10
EXP
STA
% of Cells
LAG10_UNT
LAG10_MEM
EXP_UNT
EXP_MEM
STA_UNT
STA_MEM
Cell states
Ribosome_biogenesis
LAG_EXP_transition
Respiration
Cell_division
Iron_transport
Hfq
MGE
Starvation_adaptation
Heat_shock
OsmB
Iron_transport_Heat_shock
f
MGH66: PosmB:gfp
MGH66: PrpoS:gfp
Count
Untreated
Meropenem
Green fluorescence intensity
g
MGH66:PosmB:gfp
0.034
0.0173
OsmB.high
OsmB.low
Unsorted
MGH66:PrpoS:gfp
0.043
0.027
RpoS.high
RpoS.low
Unsorted
h
Heat shock
0.0257
Survival (%)
No_pretreatment
Heat shock
i
LAG10
EXP
STA
Dominant initial cell states
Ribosome biosynthesis
Respiration
Starvation adaptation
Emerging cell states under MEM
Heat shock
OsmB
Starvation adaptation
Persistence

Figure 2. Growth-phase-specific transcriptional reprogramming under meropenem reveals divergent stress responses co-contributing to antibiotic survival.
a, UMAP embedding of single-cell transcriptomes from six conditions: three untreated (UNT) samples at early lag (10 minutes post-transfer to fresh medium, LAG10), exponential (EXP), and stationary phases (STA) and three meropenem-treated (MEM) samples collected from each corresponding growth phase (LAG10_MEM, EXP_MEM, and STA_MEM). Each condition includes two independent biological replicates (n = 2).
b, Same UMAP as in **a**, colored by transcriptional cell states. In addition to the eight shared states identified in untreated cells, three new states induced by meropenem treatment were identified: Heat shock, OsmB, and Iron transport + Heat shock.
c, Dot plot showing representative marker genes for the three meropenem-induced cell states and the Starvation adaptation cell state.
d, UMAPs of meropenem-treated cells alone, separated by growth phase. The percentage of cells in each state is labeled to highlight dominant and minor transcriptional responses (Pink, Starvation adaptation; red, Heat shock; purple, OsmB; brown, Iron transport + Heat shock)
e, Bar plot showing the distribution of all cell states, including the eight original states and three new states, across meropenem-treated samples. Percentages represent the average from two biological replicates.
f, Flow cytometry validation of scRNA-seq-inferred heterogeneity using GFP reporter strains. Promoters of *osmB* or *rpoS* were used to drive GFP expression in *K. pneumoniae* MGH66. Variable fluorescence intensity confirms heterogeneous expression across the population. This experiment was performed using three independent biological replicates (n = 3), and the data from one representative replicate is shown.
g, Functional validation of marker genes using fluorescence-activated cell sorting (FACS). EXP-phase cells with high GFP expression (top 10%) for *osmB* (OsmB.high) or *rpoS* (RpoS.high) were sorted and compared to low-expression (bottom 10%) and unsorted populations. Following 4-hour meropenem treatment (2 μg/ml), high-expressing cells showed increased survival, indicating that *osmB* and *rpoS* contribute to cell survival. Three independent biological replicates were performed (n =3). Bar plots show means of three biological replicates, and error bars represent standard deviation. Student's t-test was used for the statistical analysis *p* -values are indicated on the plot.
h, Heat shock preconditioning enhances survival under meropenem. EXP-phase cells were pre-treated at 42°C for 30 min prior to antibiotic exposure. Pre-treated cells exhibited higher survival compared to controls, supporting a protective role for heat shock priming. This experiment was performed with three biological replicates (n = 3). Bar plots show means ± standard deviation. Student's t-test was used for the statistical analysis and *p* -values are indicated on the plot.
i, Schematic model illustrating meropenem-induced persistence across growth phases. Each growth phase is characterized by a dominant pre-treatment cell state that guides distinct transcriptional responses to meropenem. These include Heat shock (with and without Iron transport), OsmB, and Starvation adaptation, which together enhance survival.

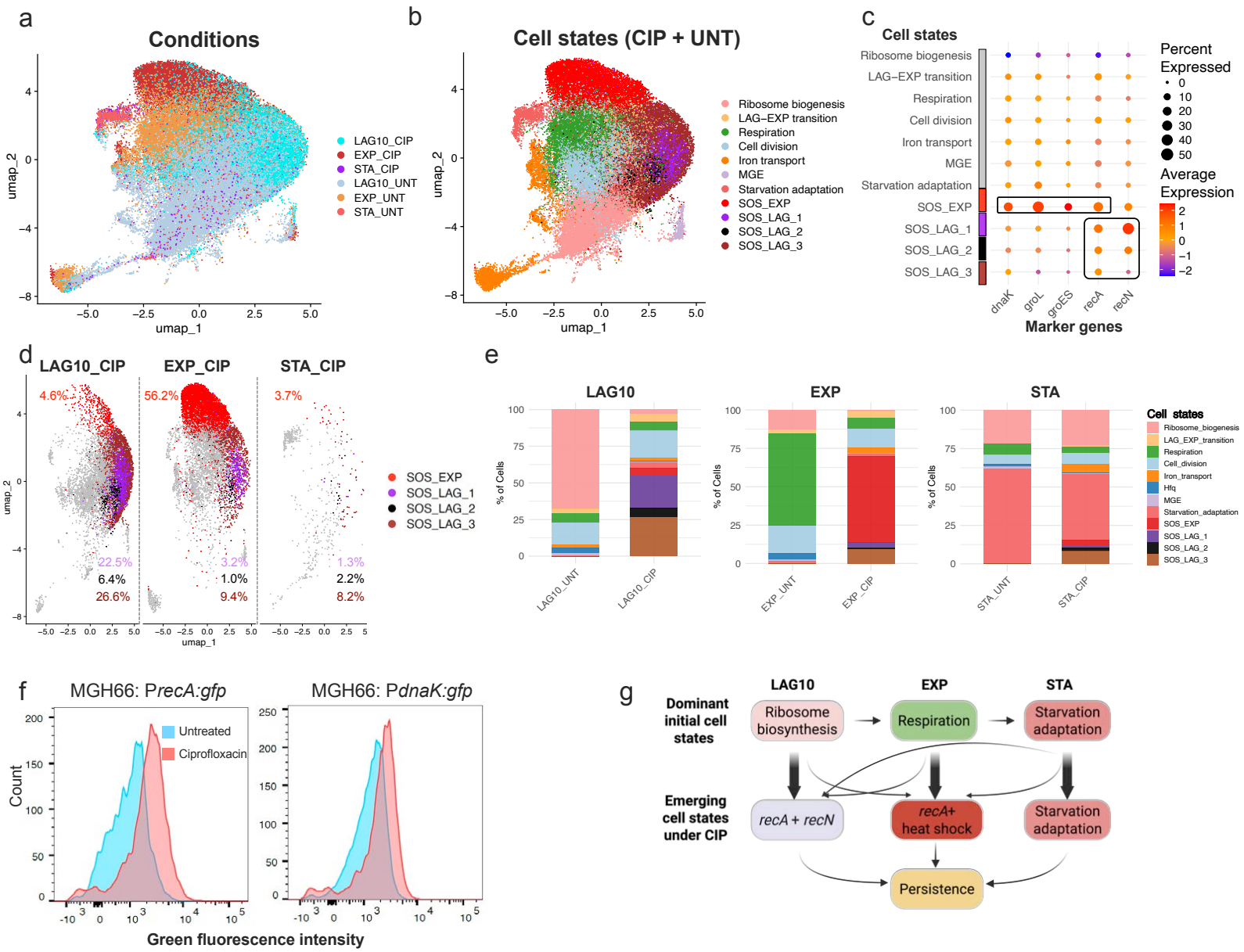
a
Conditions
umap_2
umap_1
LAG10_CIP
EXP_CIP
STA_CIP
LAG10_UNT
EXP_UNT
STA_UNT
b
Cell states (CIP + UNT)
Ribosome biogenesis
LAG–EXP transition
Respiration
Cell division
Iron transport
MGE
Starvation adaptation
SOS_EXP
SOS_LAG_1
SOS_LAG_2
SOS_LAG_3
c
Cell states
Percent Expressed
Average Expression
dnaK
groL
groES
recA
recN
Marker genes
d
LAG10_CIP
EXP_CIP
STA_CIP
4.6%
22.5%
6.4%
26.6%
56.2%
3.2%
1.0%
9.4%
3.7%
1.3%
2.2%
8.2%
e
LAG10
EXP
STA
% of Cells
LAG10_UNT
LAG10_CIP
EXP_UNT
EXP_CIP
STA_UNT
STA_CIP
Cell states
f
MGH66: PrecA:gfp
MGH66: PdnaK:gfp
Untreated
Ciprofloxacin
Count
Green fluorescence intensity
g
LAG10
EXP
STA
Dominant initial cell states
Ribosome biosynthesis
Respiration
Starvation adaptation
Emerging cell states under CIP
recA + recN
recA+ heat shock
Starvation adaptation
Persistence

Figure 3. Divergent transcriptional reprogramming is also induced under ciprofloxacin treatment.

a, UMAP embedding of single-cell transcriptomes from six conditions: three untreated (UNT) samples at early lag (10 minutes post-transfer to fresh medium, LAG10), exponential (EXP), and stationary phases (STA) and three ciprofloxacin-treated (CIP) samples collected from each corresponding growth phase (LAG10_CIP, EXP_CIP, and STA_CIP). Each condition includes two independent biological replicates (n = 2).

b, Same UMAP as in **a**, colored by transcriptional cell states. In addition to the eight shared states identified in untreated cells, four new ciprofloxacin-induced states were identified: SOS_EXP, SOS_LAG_1, SOS_LAG_2, and SOS_LAG_3, labeled based on their growth-phase origin.

c, Dot plot showing representative marker genes for the four ciprofloxacin-induced states.

d, UMAPs of ciprofloxacin-treated cells alone, separated by growth phase. The percentage of cells in each state is labeled to highlight dominant and minor transcriptional responses.

e, Bar plot showing the distribution of all cell states, including the eight shared states and four new states, across ciprofloxacin-treated samples. Percentages represent the average from two biological replicates.

f, Flow cytometry validation of scRNA-seq-inferred heterogeneity using GFP reporter strains. Promoters of *recA* or *dnaK* were used to drive GFP expression in *K. pneumoniae* MGH66. Heterogeneous fluorescence signals confirm variable expression across the population. Shown is a representative plot from three independent biological replicates (n = 3).

g, Schematic model illustrating ciprofloxacin-induced transcriptional reprogramming. Each growth phase is characterized by a dominant pre-treatment cell state, which shapes distinct stress responses upon ciprofloxacin exposure.

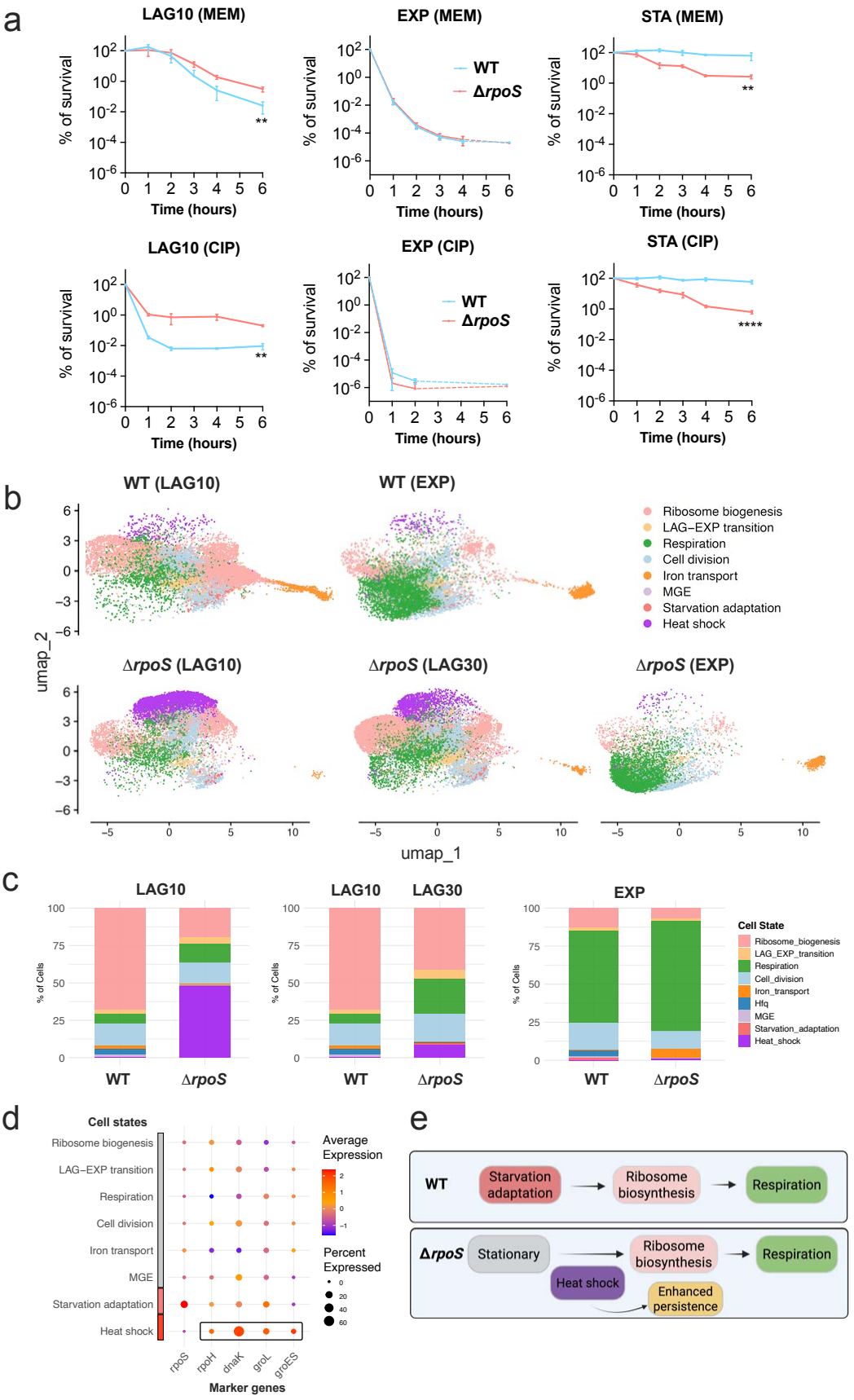
a
LAG10 (MEM)
EXP (MEM)
STA (MEM)
LAG10 (CIP)
EXP (CIP)
STA (CIP)
% of survival
Time (hours)
WT
ΔrpoS
**
****
b
WT (LAG10)
WT (EXP)
ΔrpoS (LAG10)
ΔrpoS (LAG30)
ΔrpoS (EXP)
umap_2
umap_1
Ribosome biogenesis
LAG−EXP transition
Respiration
Cell division
Iron transport
MGE
Starvation adaptation
Heat shock
c
LAG10
LAG30
EXP
% of Cells
WT
ΔrpoS
Cell State
Ribosome_biogenesis
LAG_EXP_transition
Respiration
Cell_division
Iron_transport
Hfq
MGE
Starvation_adaptation
Heat_shock
d
Cell states
Ribosome biogenesis
LAG−EXP transition
Respiration
Cell division
Iron transport
MGE
Starvation adaptation
Heat shock
rpoS
rpoH
dnaK
groL
groES
Marker genes
Average Expression
Percent Expressed
e
WT
Starvation adaptation
Ribosome biosynthesis
Respiration
ΔrpoS
Stationary
Heat shock
Ribosome biosynthesis
Respiration
Enhanced persistence

Figure 4. RpoS deficiency alters levels of antibiotic persistence via modulation of pre-treatment cell states.

a, Antibiotic killing dynamics of wild-type (WT; blue) and Δ*rpoS* (red) strains of *K. pneumoniae* MGH66 following treatment with meropenem (MEM, top) or ciprofloxacin (CIP, bottom) at early lag (10 minutes post-transfer to fresh medium, LAG10), exponential (EXP), and stationary phases (STA). RpoS deletion reduced persistence at the STA phase, increased persistence at the LAG10 phase, and showed minimal effect at the EXP phase. Curves represent the mean of three independent biological replicates (n = 3); dashed lines indicate values under the limit of detection. Error bars indicate standard deviation. Student's t-test was used for the statistical analysis to compare CFU from two strains at 6 hours after treatment. The *p* -values are 0.0083 (LAG10, MEM), 0.0032 (LAG10, CIP), 0.0078 (STA, MEM), and <0.0001 (STA, CIP). No significant difference was identified in EXP phase.

b, UMAPs comparing single-cell transcriptional states of WT (top) and Δ*rpoS* (bottom) strains across LAG10, LAG30 (30 minutes post-transfer to fresh medium), and EXP phases. A distinct cluster of cells expressing heat shock genes emerged in the Δ*rpoS* strain at LAG10, decreased at LAG30, and was largely absent at EXP. Each condition includes two biological replicates (n = 2) except for Δ*rpoS* at EXP phase, which includes only one replicate due to a technical error during library construction.

c, Quantification of cell state frequencies from **b**. Approximately 50% of Δ*rpoS* cells were in the heat shock state at LAG10, declining to 10% at LAG30, and nearly undetectable at EXP.

d, Dot plot showing representative marker genes enriched in the heat shock cluster observed in the Δ*rpoS* strain.

e, Schematic model summarizing differences in transcriptional trajectories between WT and Δ*rpoS* strains. In WT cells, the transition from stationary phase proceeds through ribosomal biogenesis and respiration. In contrast, Δ*rpoS* cells enter a heat shock state before engaging in ribosome biogenesis. The transient heat shock state may contribute to enhanced persistence in the LAG phase observed in the Δ*rpoS* strain.

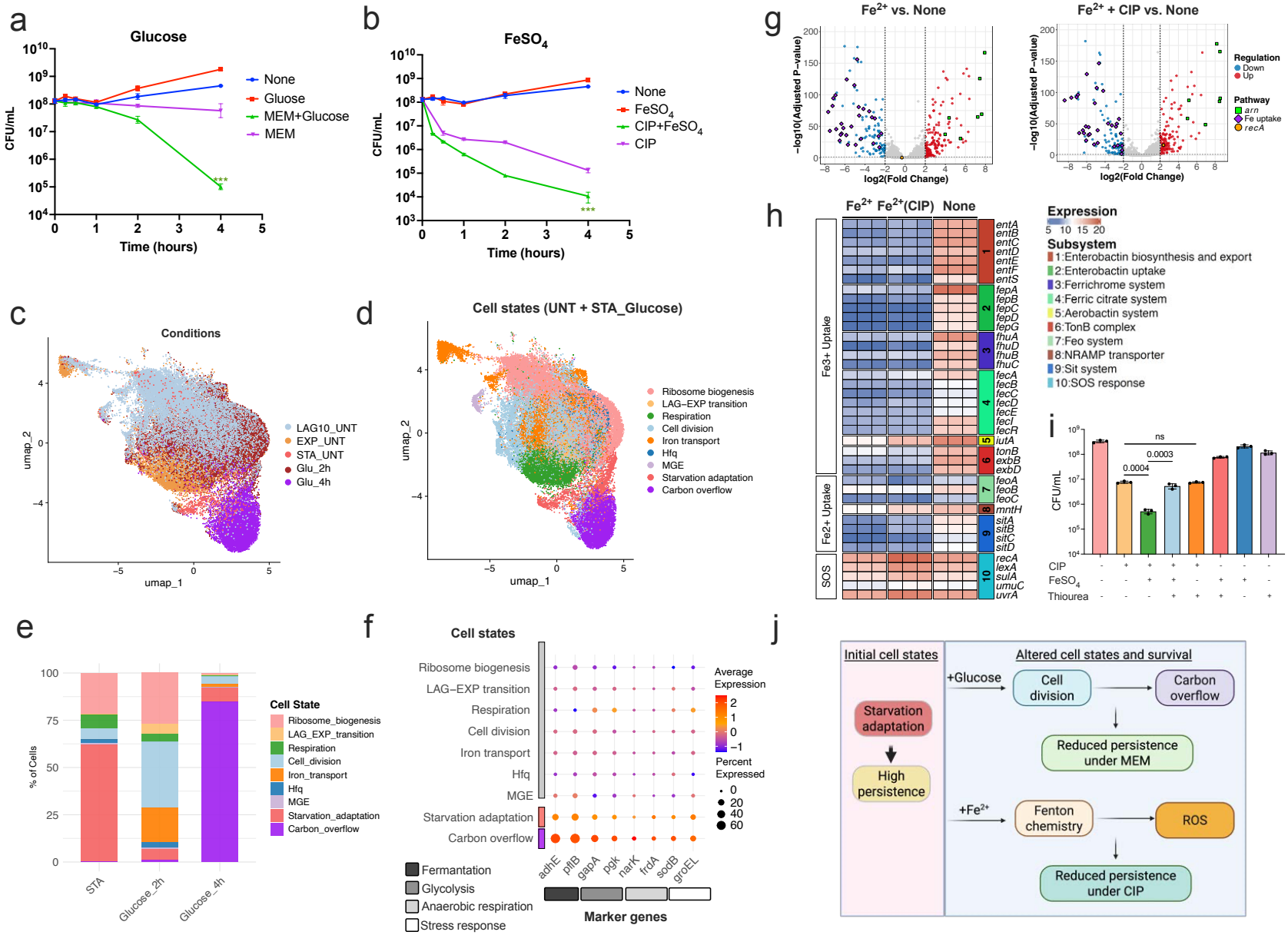
a
Glucose
CFU/mL
Time (hours)
None
Gluose
MEM+Glucose
MEM
b
FeSO4
None
FeSO4
CIP+FeSO4
CIP
c
Conditions
umap_1
umap_2
LAG10_UNT
EXP_UNT
STA_UNT
Glu_2h
Glu_4h
d
Cell states (UNT + STA_Glucose)
Ribosome biogenesis
LAG–EXP transition
Respiration
Cell division
Iron transport
Hfq
MGE
Starvation adaptation
Carbon overflow
e
% of Cells
Cell State
Ribosome_biogenesis
LAG_EXP_transition
Respiration
Cell_division
Iron_transport
Hfq
MGE
Starvation_adaptation
Carbon_overflow
STA
Glucose_2h
Glucose_4h
f
Cell states
Ribosome biogenesis
LAG–EXP transition
Respiration
Cell division
Iron transport
Hfq
MGE
Starvation adaptation
Carbon overflow
Average Expression
Percent Expressed
adhE
pflB
gapA
pgk
narK
frdA
sodB
groEL
Fermantation
Glycolysis
Anaerobic respiration
Stress response
Marker genes
g
Fe2+ vs. None
Fe2+ + CIP vs. None
−log10(Adjusted P−value)
log2(Fold Change)
Regulation
Down
Up
Pathway
arn
Fe uptake
recA
h
Fe2+ Fe2+(CIP) None
Fe3+ Uptake
Fe2+ Uptake
SOS
entA
entB
entC
entD
entE
entF
entS
fepA
fepB
fepC
fepD
fepG
fhuA
fhuD
fhuB
fhuC
fecA
fecB
fecC
fecD
fecE
fecI
fecR
iutA
tonB
exbB
exbD
feoA
feoB
feoC
mntH
sitA
sitB
sitC
sitD
recA
lexA
sulA
umuC
uvrA
Expression
Subsystem
1:Enterobactin biosynthesis and export
2:Enterobactin uptake
3:Ferrichrome system
4:Ferric citrate system
5:Aerobactin system
6:TonB complex
7:Feo system
8:NRAMP transporter
9:Sit system
10:SOS response
i
CFU/mL
ns
0.0003
0.0004
CIP
FeSO4
Thiourea
j
Initial cell states
Starvation adaptation
High persistence
Altered cell states and survival
+Glucose
Cell division
Carbon overflow
Reduced persistence under MEM
+Fe2+
Fenton chemistry
ROS
Reduced persistence under CIP

Figure 5. Nutrient shift reprograms stationary phase cells and restores antibiotic sensitivity.

a, Killing dynamics of stationary-phase (STA) *K. pneumoniae* MGH66 cells transferred to spent medium with or without 20 mM glucose, and treated with meropenem (MEM) (2 μg/ml) as indicated. Glucose supplementation significantly enhanced meropenem-mediated killing compared to meropenem alone (n = 3, $p = 0.0007$, Student's *t*-test, 4 hours).

b, Killing dynamics of STA cells transferred to spent medium with or without 10 mM $FeSO_4$, and treated with ciprofloxacin (CIP) (2.5 μg/ml) as indicated. $FeSO_4$ supplementation significantly enhanced ciprofloxacin-mediated killing compared to ciprofloxacin alone (n = 3, $p = 0.0014$, Student's *t*-test, 4 hours). Experiments in **a** and **b** were performed with three biological replicates. Curves represent the mean of three replicates; error bars denote standard deviation.

c, UMAP embedding of single-cell transcriptomes from five conditions: three untreated (UNT) samples at early lag (10 minutes post-transfer to fresh medium, LAG10_UNT), exponential (EXP_UNT), and stationary phases (STA_UNT), and two glucose-treated STA samples (STA_glucose) collected at 2 hours (Glu_2h) and 4 hours (Glu_4h) post-supplementation. Each condition includes two biological replicates (n = 2).

d, Same UMAP as in **c**, colored by transcriptional cell states. In addition to the eight shared states identified in untreated cells, glucose-treated STA cells entered a carbon overflow state at 4 hours post glucose-supplementation.

e, Bar plot showing the distribution of cell states across three conditions: STA, glucose-treated STA samples collected at 2 hours (Glucose_2h) and 4 hours (Glucose_4h) post-supplementation. Percentages represent the average from two biological replicates (n = 2).

f, Dot plot showing representative marker genes for the carbon overflow state identified in glucose-supplemented STA cells.

g, Volcano plots of bulk RNA-seq from STA cells supplemented with Fe^{2+} (10 mM), with or without ciprofloxacin (2.5 μg/ml) treatment. Fe^{2+} alone upregulated the *arn* operon and downregulated iron uptake genes. Additional ciprofloxacin treatment induced *recA*, while maintaining iron regulation changes. Genes with $\log_2$ fold change > 2 and adjusted $p < 0.05$ are highlighted. Three biological replicates were included.

h, Heatmap showing gene-level expression in Fe^{2+}- and Fe^{2+} + ciprofloxacin-treated cells. Nearly all iron uptake pathways were downregulated following Fe^{2+} supplementation, while ciprofloxacin additionally induced the SOS response.

i, Supplementation of thiourea (200 mM) significantly attenuated the Fe^{2+}-enhanced (10 mM $FeSO_4$) killing effect of ciprofloxacin (2.5 μg/ml), suggesting a role for reactive oxygen species (ROS). Three biological replicates (n = 3) were performed. CFU was quantified at 4 hours post ciprofloxacin treatment and Student's *t*-test was performed for the statistical analysis.

j, Schematic model summarizing the distinct mechanisms by which glucose and Fe^{2+} supplementation restore antibiotic sensitivity in STA cells. Glucose shifts cells from stationary phase into active division (2 hours) and carbon overflow metabolic states (4 hours), enhancing meropenem killing by reactivating the expression of drug targets. Fe^{2+} triggers Fenton chemistry, converting Fe^{2+} to Fe^{3+} and generating ROS that enhance ciprofloxacin-mediated killing. In both cases, altered initial cell states interact with drug-specific mechanisms to modulate antibiotic susceptibility.